Building Engineering 2026, 4(1), 3952.
doi: https://doi.org/10.59400/be3952

Article

Life-cycle assessment and multi-objective optimization of natural-insulated envelopes across Iranian climates

Peyman Naghipour[1,*], Afshin Naghipour[2], Tarana Bakirova[3]

[1] Department of Architecture, Ta.C., Islamic Azad University, Tabriz, Iran
[2] Department of Civil Engineering-Civil, Ta.C., Islamic Azad University, Tabriz, Iran
[3] Graphic and Media Design Department, Design Faculty, Azerbaijan University of Architecture and Construction, Baku, Azerbaijan
*** Corresponding author:** Peyman Naghipour, peyman.naghipour@yahoo.com or peyman.naghipour@iau.ir

CITATION

Naghipour P, Naghipour A, Bakirova T. Life-cycle assessment and multi-objective optimization of natural-insulated envelopes across Iranian climates. Building Engineering. 2026; 4(1): 3952. https://doi.org/10.59400/be3952

ARTICLE INFO

Received: 5 January 2026
Revised: 7 February 2026
Accepted: 10 February 2026
Available online: 28 February 2026

Abstract: The building envelope plays a pivotal role in achieving sustainable energy performance, particularly in regions characterized by extreme climatic variations. This study investigates the holistic optimization of building envelopes—comprising walls, roofs, floors, and fenestrations—by integrating natural insulation materials with passive and smart design strategies. The research aims to enhance energy efficiency, reduce total CO_2 emissions, and improve occupants' thermal comfort across four representative low-income climatic regions of Iran: Yazd (hot-arid), Tabriz (cold-dry), Rasht (temperate-humid), and Bandar Abbas (hot-humid). Addressing the existing research gap, the study extends beyond operational energy analysis by incorporating a full life cycle assessment (LCA), including embodied energy and life cycle carbon footprint. Multi-objective optimization (using NSGA-II) was performed to minimize annual energy demand, life-cycle cost (LCC), and environmental impact simultaneously. Building performance simulations were conducted using IES-VE and EnergyPlus, while LCA and economic analyses were executed via SimaPro and HOMER Pro. The results indicate that hybrid natural insulations-particularly straw–hemp composites-combined with passive strategies (dynamic shading, natural ventilation, and thermal mass enhancement) can reduce total CO_2 emissions by 42–58% compared with conventional materials. Also, the results demonstrate that the optimized design solutions can reduce annual energy consumption by approximately 25–35% compared to the baseline design, while achieving a 15–25% reduction in life-cycle costs over the building lifespan. Additionally, orientation-sensitive optimization improved thermal comfort indices (Predicted Mean Vote—PMV, Predicted Percentage of Dissatisfied—PPD) throughout the year. The developed predictive models based on machine learning (Random Forest) exhibited robust accuracy in estimating energy consumption. The findings provide an integrated framework for sustainable, low-cost, and climate-responsive envelope design, supporting the transition toward net-zero energy buildings in developing regions.

Keywords: life-cycle assessment; multi-objective optimization; natural insulation; Iranian climates; operational energy; embodied carbon

1. Introduction

In recent years, the building envelope has moved to the center of global decarbonization debates because it governs the dominant pathways of heat and moisture exchange that drive space-conditioning energy in housing, especially across climates

with pronounced seasonal and diurnal swings [1,2]. In developing contexts where rapid urbanization collides with cost constraints and material supply chains, envelope choices become a first-order lever for lowering operational energy, curbing life-cycle carbon, and safeguarding thermal comfort for vulnerable households [3, 4]. Framed against national carbon-neutrality ambitions and the rising frequency of extreme heat events, a climate-responsive, life-cycle-aware approach to envelope design is no longer optional but essential for equitable, low-cost mitigation [5,6].

A growing body of literature has explored insulation enhancement, glazing optimization, and façade geometry tuning using dynamic simulation tools and, more recently, data-driven surrogates [7, 8]. Studies report sizable savings from improved U-values, reflective roofs, and optimal window-to-wall ratios (WWR), yet often consider a single component (typically walls) or a single climate, limiting transferability [9–11]. Parallel research has advanced bio-based insulations (e.g., straw, hemp, cork, and cellulose) as eco-efficient alternatives to petrochemical products, documenting low embodied energy and carbon sequestration potential [12–14]. However, many assessments remain circumscribed to temperate settings, with limited evidence for hot-arid or hot-humid regimes, and frequently evaluate operational energy in isolation, overlooking embodied burdens and end-of-life impacts [15–18]. Optimization efforts commonly compare a handful of predefined assemblies rather than resolving trade-offs among energy, carbon, and cost on Pareto fronts [19, 20]. Machine-learning accelerators have emerged to reduce computational expense but are rarely coupled to full envelope configurations with natural materials across multiple climates [21,22].

Consequently, several gaps persist. First, a fragmented scope underestimates cross-component interactions among walls, roofs, floors, and fenestrations, where hygrothermal couplings and solar-optical effects can amplify or offset one another [23,24]. Second, the omission of life-cycle thinking risks favoring ostensibly efficient solutions whose embodied carbon negates operational gains [25–27]. Third, evidence from extreme and composite climates remains sparse, impeding generalizable guidance for regions like Iran that span hot-arid, cold-dry, temperate-humid, and hot-humid conditions [28–30]. Fourth, multi-objective formulations that jointly minimize annual energy, life-cycle cost (LCC), and life-cycle carbon remain underused, and few studies fuse such optimization with surrogate learning for speed and interpretability [31–34].

In practice, designers of low-income residential buildings face critical constraints that go beyond theoretical energy optimization targets [35–37]. These constraints primarily include the affordability, local availability, and constructability of building materials, which significantly limit the applicability of many advanced sustainable design strategies. While previous studies have extensively addressed energy efficiency and environmental performance [38, 39], fewer have explicitly integrated material affordability and accessibility as decisive parameters in the early design stage of low-income housing [40, 41]. Therefore, this research explicitly links the identified

research gaps to real-world design challenges by incorporating cost-sensitive and locally available insulation materials into the optimization framework. This approach ensures that the proposed solutions are not only environmentally and energetically efficient but also practically feasible for designers working under budgetary and material constraints typical of low-income housing projects. Consequently, the proposed integrated framework bridges the gap between advanced computational optimization techniques and the practical realities of low-income housing design, offering a multidisciplinary, cost-aware, and computationally efficient decision-support tool for designers.

Therefore, this study advances a unified framework that (i) models the complete envelope-walls, roofs, floors, and fenestrations-under four representative Iranian climates (cities of Yazd, Tabriz, Rasht, Bandar Abbas), (ii) compares natural and conventional insulations within a cradle-to-grave Life Cycle Assessment (LCA), and (iii) applies multi-objective optimization (e.g., NSGA-II) to resolve energy–carbon–cost trade-offs while enforcing comfort constraints (PMV/PPD). The framework is further accelerated and explained through machine-learning surrogates (e.g., Random Forest) trained on simulation outputs to deliver rapid prediction and feature-level insight. The novelty lies in the envelope-wide scope, the explicit coupling of dynamic comfort with life-cycle carbon and LCC, and the integration of surrogate-assisted optimization to expose interpretable Pareto solutions tailored to climate diversity and affordability.

Now, this research seeks to answer the following questions:

1– How do natural insulation systems compare with conventional materials in reducing annual energy and total life-cycle CO_2 across hot-arid, cold-dry, temperate-humid, and hot-humid zones?

2– To what extent does integrating LCA (embodied + operational) alter “optimal” envelope selections relative to energy-only evaluations?

3– Which Pareto-optimal configurations best balance energy, carbon, and LCC while satisfying thermal comfort constraints?

4– Can machine-learning surrogates trained on physics-based simulations accurately and transparently predict energy and carbon outcomes to support design decisions?

The remainder of this paper is organized as follows:

- Section 2 synthesizes prior work on envelope performance, natural insulations, LCA, optimization, and ML in building energy.
- Section 3 details the simulation setup, life-cycle, multi-objective optimization formulation, and surrogate modeling workflow.
- Section 4 reports results for climate-specific performance, trade-offs, and model interpretability.
- Section 5 discusses mechanisms, policy and design implications, and limitations.
- Section 6 concludes with key contributions and future research directions.

2. Literature review

2.1. Introduction to the literature review

A coherent understanding of how building envelopes influence energy performance, environmental impacts, and occupants' comfort is essential for positioning the present research within the broader field. The literature on envelope design, natural insulation, life-cycle assessment (LCA), and multi-objective optimization has expanded rapidly, yet it remains fragmented across disciplines. A structured review is therefore required to clarify what has been achieved, to critically assess the methodological limitations of previous studies, and to identify the specific gaps that justify a combined life-cycle and multi-objective approach for climate-responsive envelopes in Iranian contexts.

2.2. Thematic synthesis of previous studies

2.2.1. Conventional envelope design and energy efficiency

Early research on building envelopes focused predominantly on reducing operational energy by improving thermal resistance of individual components, especially walls. Static or steady-state models were frequently used to examine the influence of conventional insulations such as expanded polystyrene (EPS), polyurethane foam, and mineral wool on heating and cooling loads [42]. These studies showed that increasing insulation thickness and lowering U-values can substantially reduce heat losses and annual energy demand [43–45]. However, they typically treated envelope elements in isolation, often concentrating on walls and neglecting roofs, floors, and fenestrations as interacting subsystems. This reductionist treatment limited the understanding of cross-component thermal interactions and their implications for whole-building performance.

With the advent of dynamic building performance simulation (BPS) tools such as EnergyPlus, IES-VE, and DesignBuilder, research moved towards time-resolved analyses driven by climatic data [46–48]. These dynamic simulations enabled a more realistic representation of transient heat transfer, solar gains, and occupant-related internal loads. Studies using such tools systematically varied envelope parameters-insulation type, wall composition, window-to-wall ratio (WWR), glazing characteristics-and confirmed that optimized configurations may lead to notable reductions in annual heating and cooling energy [49–51]. Yet, most of these contributions still emphasized operational performance alone and rarely evaluated the environmental or economic implications of alternative envelope assemblies over the full life cycle.

2.2.2. Natural insulation materials and environmental performance

In response to concerns about embodied energy, fossil-based materials, and waste generation, attention has increasingly shifted toward bio-based and natural insulation materials such as hemp, kenaf, flax, cork, cellulose, and agricultural residues [52]. Experimental and numerical studies report that these materials can achieve thermal conductivities comparable to or only slightly higher than those of mineral wool

or EPS, while offering lower embodied carbon due to renewable feedstocks and potential carbon sequestration during growth [53, 54]. For example, hemp-lime and wood-fiber composites have been shown to deliver competitive thermal resistance with significantly reduced life-cycle greenhouse gas emissions.

However, the adoption of natural insulation remains constrained by several technical and contextual factors. Reported performance varies widely due to differences in density, moisture content, and manufacturing processes [55]. Furthermore, hygrothermal behavior, long-term durability, and vulnerability to biological degradation are not yet fully understood, particularly in hot-arid and hot-humid environments. Much of the existing evidence is derived from temperate or Mediterranean climates, and only a limited number of studies consider extreme temperature swings or high humidity typical of many regions in the Global South. As a result, the robustness of natural insulation systems under diverse climatic loads, especially in low-income housing, remains insufficiently documented.

2.2.3. Life-cycle assessment of envelope systems

Parallel to material-focused research, Life Cycle Assessment has become a mainstream methodology for evaluating the environmental performance of buildings and their components. LCA studies have demonstrated that while operational energy historically contributed the largest share of total emissions, the relative importance of embodied impacts increases as buildings become more energy efficient [56, 57]. Several comparative LCAs have contrasted natural and conventional insulation systems, revealing that bio-based products can reduce life-cycle CO_2 by 30–45% when sourced locally and designed for end-of-life recovery or reuse [58].

Despite these advances, the integration of LCA with dynamic energy simulation in envelope studies remains partial. Methodological inconsistencies across databases, limited regional data, and simplified end-of-life scenarios introduce uncertainty into comparative assessments [59]. Many studies compute embodied impacts separately from operational energy, rather than embedding LCA-derived metrics into an integrated design and optimization process. Consequently, envelope solutions may be labeled “optimal” based on energy savings alone, even when their embodied carbon substantially offsets operational gains.

2.2.4. Multi-objective optimization of envelope performance

As the number of design variables and performance criteria has increased, researchers have adopted multi-objective optimization (MOO) algorithms to explore trade-offs among energy, cost, and environmental indicators. Population-based techniques such as Genetic Algorithms (GA), NSGA-II, and Multi-Objective Particle Swarm Optimization (MOPSO) have been widely employed to construct Pareto fronts for envelope configurations [60]. When coupled with BPS tools, these algorithms can systematically search combinations of insulation thickness, glazing type, WWR, roof reflectivity, and orientation to identify sets of non-dominated solutions that balance competing objectives such as annual energy demand and life-cycle cost [61, 62].

Nevertheless, several limitations persist. In many studies, optimization is carried out for a single climate or building archetype, which restricts the generalizability of

results. Environmental indicators such as life-cycle carbon are either omitted or treated in a simplified way, and natural insulation materials are rarely included as explicit design options. Moreover, MOO is often applied to a narrow subset of envelope components, e.g., walls and windows, without considering the combined effects of roofs and floors. As a result, cross-component synergies and trade-offs among operational energy, life-cycle emissions, and economic feasibility are not fully captured [63].

2.2.5. Machine-learning-assisted prediction and optimization

Machine learning has recently emerged as a powerful complement to physics-based simulation in building energy research. Algorithms such as Random Forests, Support Vector Machines, artificial neural networks, gradient boosting, and CatBoost have been trained on simulated or measured datasets to predict heating and cooling loads based on geometric, material, and climatic features [64, 65]. These models offer two main advantages: they can approximate complex nonlinear relationships at a fraction of the computational cost of full BPS, and many of them provide measures of feature importance that support interpretability [66,67].

Hybrid frameworks that embed ML surrogates within optimization loops have been shown to accelerate convergence by replacing most expensive simulation calls with rapid predictions. However, only a limited number of studies have applied such surrogate-assisted optimization to full envelope configurations that explicitly include natural insulation materials, and even fewer have extended analyses across multiple climatic zones. In addition, ML models are often developed solely for load prediction, without explicit coupling to life-cycle carbon or cost metrics, which constrains their usefulness for comprehensive sustainable design.

2.2.6. Passive design, renewables, and socio-economic context

Beyond material choices, passive strategies-dynamic shading, natural ventilation, thermal mass enhancement-and on-site renewable systems (e.g., photovoltaic panels) have been combined with envelope optimization to further reduce energy use and peak loads [68, 69]. Case studies report cooling demand reductions of up to 30% when high-performance envelopes are complemented by properly controlled shading and night ventilation in warm climates. Nonetheless, many of these investigations remain at prototype or demonstration scale, with limited attention to cost, affordability, or local supply chains.

Crucially, the socio-economic dimension is often weakly represented. Few studies explicitly target low-income housing or evaluate the feasibility of natural insulation systems considering local availability, construction practices, and household energy budgets [70,71]. This lack of contextualization limits the practical transfer of technical findings into policies and design guidelines for vulnerable communities in developing regions.

2.3. Research gap identification

A critical synthesis of the above strands reveals several interrelated research gaps that motivate the present study:

1. **Fragmented envelope scope.** Many investigations restrict the analysis to a

single component—most commonly wall insulation—while neglecting roofs, floors, and fenestrations or treating them with simplified assumptions [72, 73]. This fragmented treatment overlooks hygrothermal couplings and solar-optical interactions that can amplify or offset each other at whole-envelope scale.

2. **Incomplete life-cycle integration.** A substantial body of work optimizes envelopes based solely on operational energy, ignoring embodied energy and carbon associated with material production, transportation, and end-of-life stages [74]. Without full life-cycle integration, envelope designs may appear favorable in terms of annual energy demand while performing poorly in total carbon footprint.
3. **Limited climatic coverage and contextual relevance.** Existing studies are heavily concentrated in European and Mediterranean climates, with comparatively little evidence from hot-arid, cold-dry, temperate-humid, and hot-humid regions typical of Iran and many other developing countries [75]. The lack of multi-climatic analyses constrains the derivation of robust design guidelines for nations with pronounced climatic diversity.
4. **Underdeveloped multi-objective and multi-criteria frameworks.** Although MOO techniques are now widely available, relatively few envelope studies formulate optimization problems that simultaneously minimize energy use, life-cycle carbon, and life-cycle cost while enforcing thermal comfort limits [76, 77]. The combined evaluation of environmental and economic performance, especially for natural insulation systems, therefore remains underexplored.
5. **Limited use of artificial intelligence for envelope-wide, life-cycle-aware design.** Machine-learning models have mainly been deployed for short-term load prediction or for accelerating single-objective optimization. Their application to envelope-wide, climate-diverse, and life-cycle-informed design spaces—particularly including natural insulation materials—has been scarce [78].
6. **Insufficient socio-economic grounding.** Very few studies explicitly address affordability, local material availability, or implementation barriers in low-income housing contexts, even though these factors ultimately determine the real-world adoption of sustainable envelope solutions [79].

Together, these gaps indicate a need for research that concurrently: (i) considers the complete envelope system, (ii) integrates operational and embodied impacts, (iii) spans multiple climatic conditions, (iv) adopts a rigorous multi-objective formulation, and (v) leverages interpretable ML surrogates, all within a socio-economically relevant context.

2.4. Rationale and conceptual framework for the present study

To address these gaps, the present study proposes an integrated framework that couples dynamic simulation, life-cycle assessment, multi-objective optimization, and machine-learning surrogate modeling for complete residential envelopes in four representative Iranian climates. The rationale rests on four complementary layers.

First, an **envelope simulation layer** models walls, roofs, floors, and fenestrations using IES-VE and EnergyPlus to capture transient thermal behavior, HVAC loads,

and comfort indices (PMV, PPD) under realistic meteorological conditions for Yazd (hot-arid), Tabriz (cold-dry), Rasht (temperate-humid), and Bandar Abbas (hot-humid). This holistic representation explicitly includes cross-component interactions that are often neglected in wall-centric studies.

Second, a **sustainability assessment layer** extends the analysis from operational energy to embodied impacts by performing cradle-to-grave LCA for both natural and conventional insulation systems using tools such as SimaPro or OneClick LCA. This layer quantifies embodied energy and life-cycle CO_2, enabling consistent comparison of material alternatives across climates and envelope configurations.

Third, an **optimization layer** formulates a three-objective problem that simultaneously minimizes annual operational energy, total life-cycle carbon, and life-cycle cost while enforcing comfort and payback constraints. NSGA-II (or similar evolutionary algorithms) is used to generate climate-specific Pareto fronts and to reveal trade-offs among energy, environmental, and economic goals that are directly relevant for low-income housing.

Fourth, a **predictive intelligence layer** employs machine-learning models (e.g., Random Forest or other ensemble methods) trained on simulation outputs to serve as fast, interpretable surrogates. These models are subsequently embedded into the optimization process to drastically reduce computational effort and to provide feature-level insights into the relative importance of envelope and climate variables.

By combining these layers, the study responds directly to the identified research gaps: it treats the envelope as an integrated system, embeds LCA and LCC into the optimization, examines multiple extreme and composite climates relevant to Iran, and exploits interpretable ML to support rapid yet transparent design exploration.

2.5. Summary of the literature review

In summary, the literature indicates substantial progress in optimizing building envelopes for energy efficiency, exploring natural insulation materials, and applying LCA, MOO, and ML techniques. However, prior work remains fragmented across components, limited in climatic diversity, and frequently restricted to operational energy or single-objective formulations. The role of natural insulation in full life-cycle, multi-objective envelope optimization-especially for low-income housing in climates such as those of Yazd, Tabriz, Rasht, and Bandar Abbas-has been insufficiently investigated.

These shortcomings motivate the present research, which develops and applies an integrated, envelope-wide framework that combines dynamic simulation, cradle-to-grave environmental and economic assessment, surrogate-assisted multi-objective optimization, and interpretable machine learning. In doing so, the study seeks to provide evidence-based guidance on how natural insulation systems can be configured to balance energy demand, life-cycle carbon, and cost while maintaining acceptable comfort across diverse Iranian climates, thereby addressing both scientific and practical needs in sustainable envelope design.

3. Methodology

This study employed an integrated experimental–computational framework to evaluate, optimize, and predict the performance of complete residential building envelopes incorporating natural-fiber insulation. The approach combined dynamic whole-building simulation, life-cycle assessment (LCA), multi-objective optimization, and machine-learning surrogate modeling within a single workflow. The end-to-end process—from data generation and simulation through life-cycle analysis, optimization, and explainable AI—is summarized in **Figure 1**, while **Figure 2** shows the four representative Iranian climates that anchored all scenarios.

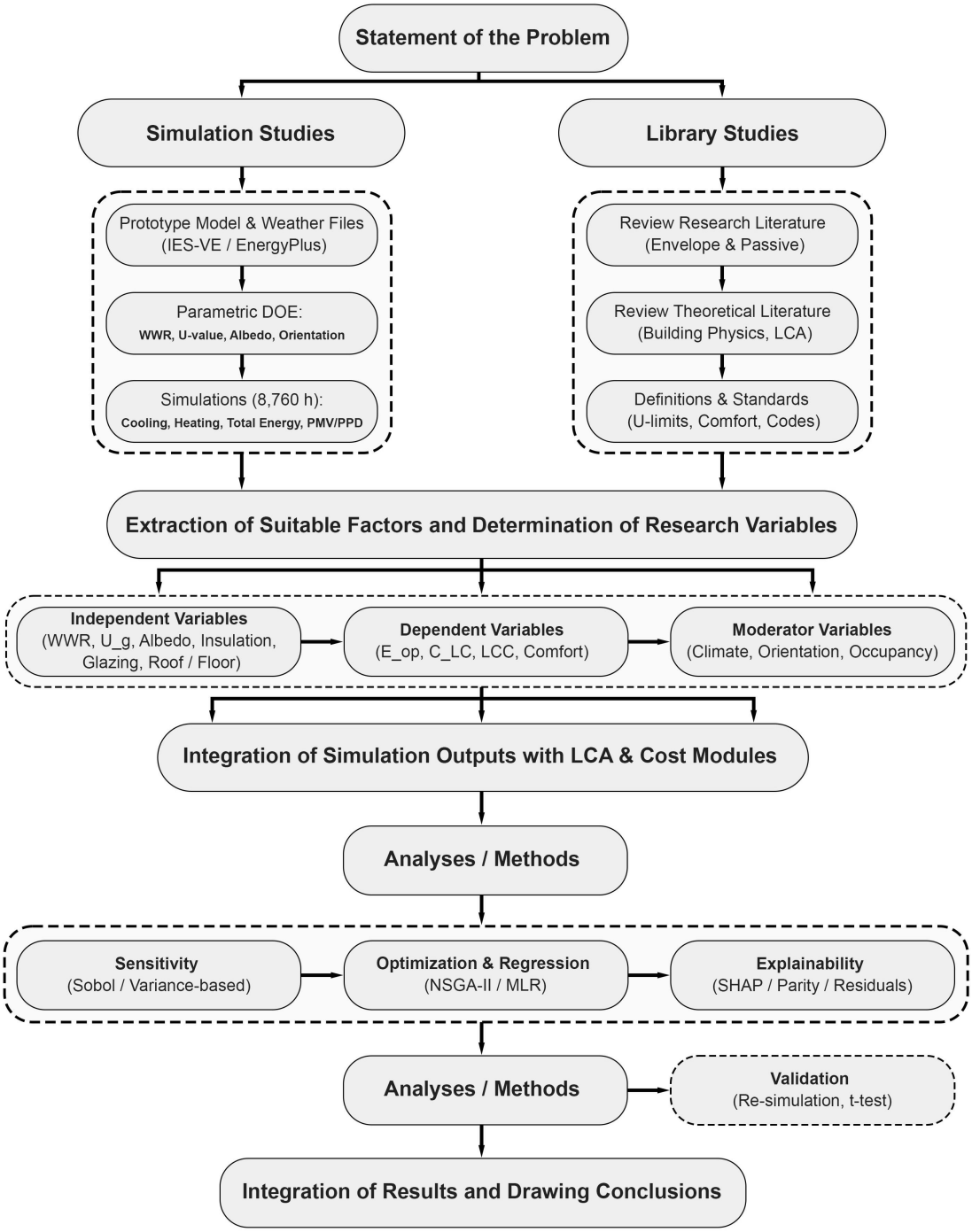

Figure 1. End-to-end methodological framework.

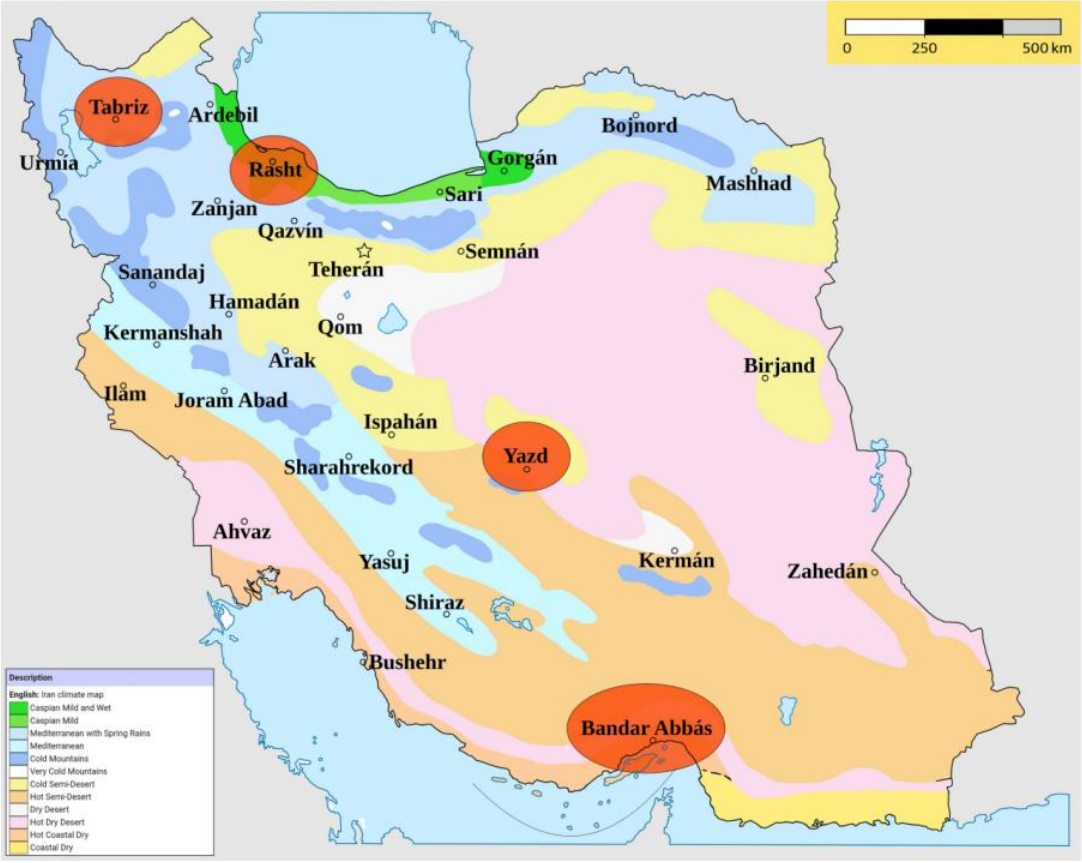

Figure 2. Determining climatic locations on the map of Iran.

3.1. Research design, study area, and building prototype

The research was designed as a simulation-based parametric study with life-cycle and economic extensions. Four representative cities were selected to capture the main climatic typologies of Iran: Yazd (hot–arid), Tabriz (cold–dry), Rasht (temperate–humid), and Bandar Abbas (hot–humid), as illustrated in **Figure 2**. These locations span extreme and composite conditions typical of low-income housing contexts and thus provide a robust testbed for evaluating climate-responsive envelope strategies.

A prototypical single-story residential dwelling with a conditioned floor area of 80 m^2 was adopted as the reference building. The floor plan, envelope layout, and opening positions were based on a typical low-income housing module documented in the local literature and practice. The envelope was decomposed into four principal component types: external walls, roof, floor slab, and fenestration systems. Each component was represented as a multi-layer assembly whose thermal and hygrothermal behavior was explicitly modeled (**Figure 3**).

To ensure reproducibility, all simulations were implemented using IES-VE and EnergyPlus (functionally equivalent dynamic engines), with post-processing and model management performed in Python 3.x. LCA calculations were carried out in SimaPro, while life-cycle cost and energy-related economic analyses were supported by HOMER Pro. Optimization and machine-learning routines were coded in Python using standard scientific libraries (NumPy, SciPy, scikit-learn).

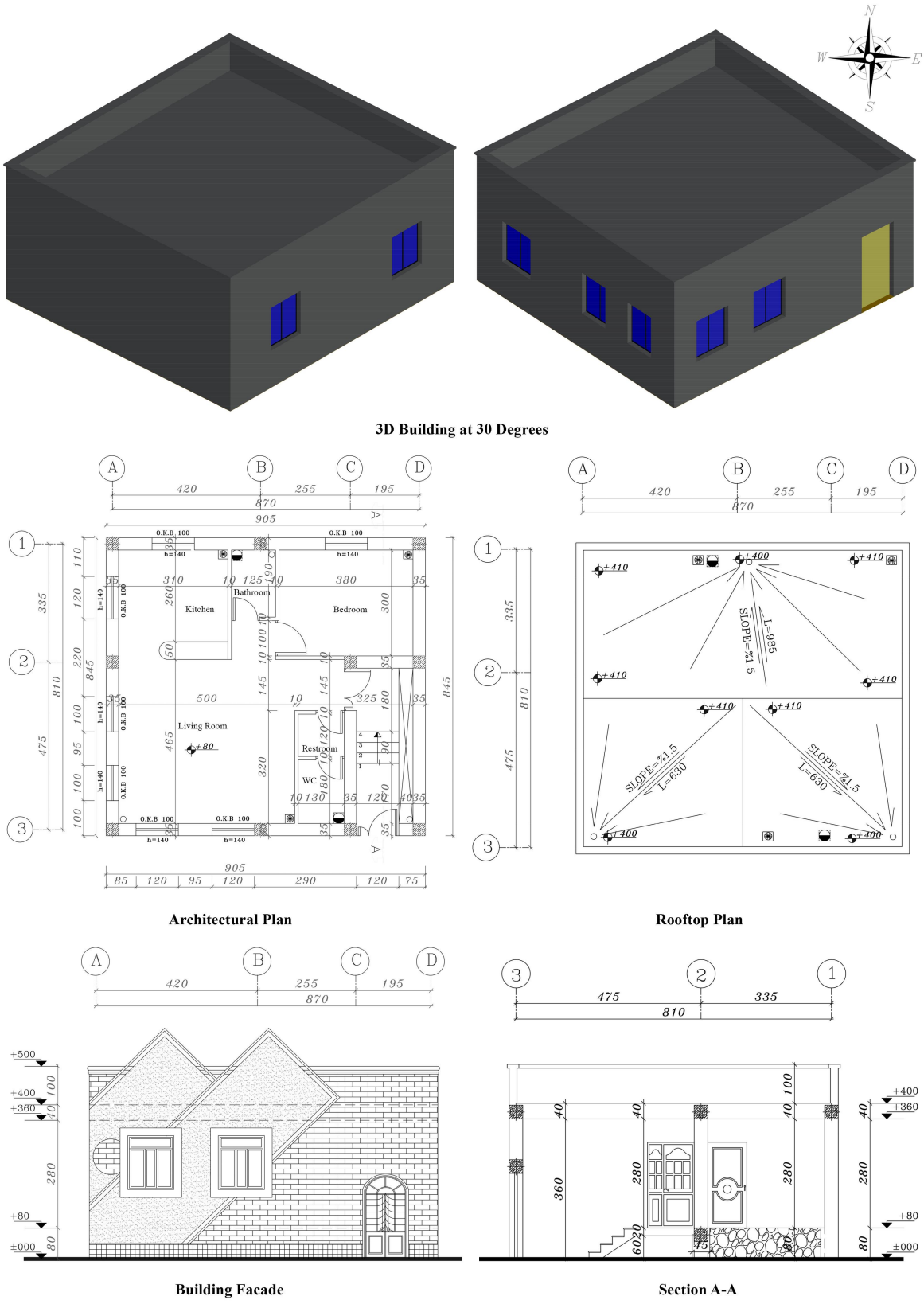

Figure 3. 3D schematic of the building along with architectural plan, rooftop, facade and section A-A.

3.2. Data generation and simulation setup

The overall analytical framework adopted in this study is designed to ensure methodological rigor through systematic data collection, full-factorial sampling, and

dynamic performance simulation. The combined use of IES-VE and EnergyPlus enables accurate modeling of building energy behavior under varying design configurations. Furthermore, the integration of NSGA-II for multi-objective optimization and Random Forest–based surrogate modeling ensures both robustness and computational efficiency in evaluating energy use intensity (EUI) and life-cycle cost (LCC).

3.2.1. Envelope materials and property database

For each envelope component, a material library was defined that included both natural and conventional insulation options. The natural insulation set comprised kenaf, hemp, wood fiber, pineapple fibers, rice husk, and cotton-stalk-based products, while mineral wool and expanded polystyrene (EPS) were used as conventional benchmarks. For each material, thermal conductivity k, bulk density ρ, specific heat capacity c_p vapor diffusion resistance factor μ, and, where relevant, sound absorption coefficient were collected from experimental datasets and technical reports. The resulting property database, used consistently across all climates and simulations, is summarized in **Table 1**.

Table 1. Material thermal and hygrothermal properties.

Material	***k* (W·m⁻¹·K⁻¹)**	***ρ* (kg·m⁻³)**	***c_p* (J·kg⁻¹·K⁻¹)**	***μ* (−)**	**α_sound**
Kenaf	0.044	180	1700	2.3	0.95
Pineapple	0.057	232	1890	4.9	0.9
Wood fiber	0.05	270	2100	5	0.32
Hemp	0.123	100	1800	10	0.6
Mineral wool	0.036	35	840	1	0.4
EPS	0.033	20	1400	1	0.25

Note: Real dataset used in simulations.

This library enabled systematic comparison of bio-based and petrochemical-based insulations under the same geometric and climatic conditions, avoiding confounding effects from inconsistent data sources.

3.2.2. Dynamic simulation environment and boundary conditions

Dynamic energy simulations were carried out using a whole-building performance engine (IES-VE/EnergyPlus equivalent), in which transient heat conduction through each layered envelope element was governed by the one-dimensional heat transfer equation [80]:

$$\rho c_p \frac{\partial T(x,t)}{\partial t} = \frac{\partial}{\partial x}\left(k\frac{\partial T(x,t)}{\partial x}\right) + q'''(x,t) \tag{1}$$

as expressed in Equation (1). Here, ρ denotes density, c_p specific heat, k thermal conductivity, and q''' the volumetric heat source term. The governing equation was discretized by finite differences in space (Δx) and an implicit time-stepping scheme (Δt) leading to the matrix formulation in Equation (2) [81]. This scheme ensured numerical stability under hourly climatic forcing.

$$\mathrm{C}\frac{\mathrm{T}^{n+1}-\mathrm{T}^{n}}{\Delta t} + \mathrm{K}\mathrm{T}^{n+1} = \mathrm{Q}^{n+1} \tag{2}$$

Boundary conditions at internal and external surfaces included convective heat transfer, longwave and shortwave radiation exchange, and standard infiltration and ventilation rates appropriate for residential buildings. Internal gains from occupants, lighting, and appliances were represented using three distinct occupancy schedules to capture realistic variations in use patterns.

Typical meteorological year (TMY) datasets for Yazd, Tabriz, Rasht, and Bandar Abbas were used to drive the simulations. For each configuration, annual operational energy demand for space conditioning, E_{op}, was computed by integrating the hourly HVAC power consumption P_{hvac} *(h)* over one year, as defined in Equation (3) [82]. This quantity served as the primary operational performance indicator.

$$E_{op} = \sum_{h=1}^{8760} P_{hvac}(h) \cdot \Delta t \tag{3}$$

where $P_{hvac}(h)$ is HVAC power at hour h.

For reporting and all statistical/ML analyses, operational energy *E_op* is converted to energy use intensity (EUI) = *E_op*/A_floor and reported in kWh·m^{-2}·yr^{-1}; consequently, all error metrics (RMSE, MAE) are also reported in kWh·m^{-2}·yr^{-1}.

3.2.3. Factorial design and sample size

To explore the design space in a systematic and reproducible manner, a full-factorial sampling strategy was adopted. For each climate, all combinations of the following categorical variables were generated: six insulation options, three glazing types (with distinct U-values and solar heat gain coefficients), two roof strategies (e.g., standard vs. high-albedo coating), and two floor strategies (e.g., uninsulated vs. insulated slab). This base design yielded 72 envelope configurations per climate.

Geometric and operational variability were then introduced by combining each configuration with two building orientations (0° and 90°), three WWR levels (10%, 25%, 40%), and three occupancy schedules. The resulting design matrix comprised approximately [83]: 72 × 4 climates × 3 WWR × 2 orientations × 3 schedules ≈ 5184.

Simulated annual cases. The structure of this design and the associated factor levels are summarized in **Table 2**, while **Figure 3** illustrates the building geometry and envelope components.

Table 2. Experimental design summary (how to present it).

Factor	Levels
Insulation type	6
Glazing type	3
Roof strategy	2
Floor strategy	2
WWR	3
Orientation	2
Occupancy schedule	3
Climates	4
Total cases	5184

3.3. Life-cycle assessment and performance indicators

3.3.1. Embodied and operational impacts

A cradle-to-grave LCA was performed for each envelope configuration. Embodied energy $E_{emb,i}$ and embodied carbon $C_{emb,i}$ for component i were computed by multiplying the mass of each constituent material m_{ij} by its embodied energy factor e_j and embodied carbon factor c_j, respectively, as defined in Equation (4) [84]. The required coefficients were obtained from established LCA databases and manufacturer environmental product declarations and are summarized in **Table 3**.

$$E_{emb,i} = \sum_j m_{ij} \cdot e_j \qquad C_{emb,i} = \sum_j m_{ij} \cdot c_j \tag{4}$$

Table 3. Embodied factors (sample data).

Material	*e_j* (MJ/kg)	*c_j* (kgCO₂/kg)
Kenaf	2.4	0.05
Pineapple	3.1	0.08
Wood fiber	3.6	0.09
Mineral wool	60	2.2
EPS	70	2.6

Total life-cycle carbon C_{LC} was evaluated as the sum of embodied emissions and operational emissions over the analysis horizon. Operational emissions were derived by scaling annual HVAC energy consumption with the grid emission factor EF_{grid} and system efficiency η_{grid} according to Equation (5) [85]. This formulation ensured consistent treatment of both material-related and energy-related burdens across climates and designs.

$$C_{LC} = C_{emb} + \sum_{h=1}^{8760} \left(\frac{P_{hvac}(h)}{\eta_{grid}} \right) \cdot EF_{grid} \tag{5}$$

3.3.2. Life-cycle cost

Life-cycle cost (LCC) was defined as the sum of initial investment (CAPEX), operational energy costs (OPEX), and replacement costs over the building lifetime. Unit material and installation costs were compiled from regional databases and supplier catalogs, while energy prices and discount rates reflected national averages for residential customers. The same economic assumptions were applied uniformly to all configurations to maintain comparability.

3.4. Multi-objective optimization

From a computational perspective, direct coupling of detailed building energy simulation tools with multi-objective optimization algorithms often leads to high computational costs, limiting their usability in real-world building projects. To address this challenge, this study employs machine learning–based surrogate models as an efficient alternative to repeated full-scale simulations.

Surrogate models approximate the input–output relationships of complex

energy simulations with significantly reduced computational effort, enabling faster exploration of design alternatives. This reduction in computational time is particularly advantageous for practical design scenarios, where designers require rapid feedback to evaluate multiple material and configuration options within limited project timelines. By integrating surrogate modeling within the optimization framework, the proposed methodology enhances both computational efficiency and practical applicability in actual building design processes.

3.4.1. Objective functions and decision variables

The envelope design problem was cast as a three-objective optimization task in which the following metrics were minimized simultaneously:

1. Operational energy: $f_1 = E_{op}$(kWh/yr)
2. Life-cycle carbon: $f_2 = C_{LC}$ (kgCO_2/yr or equivalent)
3. Life-cycle cost: $f_3 = LCC =$ CAPEX + OPEX + Replacement

The decision vector **x** contained discrete choices for insulation type, glazing type, roof strategy, floor strategy, WWR level, and orientation, as expressed in Equation (6) [86]. These variables were optimized subject to technical and comfort constraints, including a maximum wall U-value, a PMV range of [−0.5,+0.5], and a simple payback limit of 20 years (Equation (7)) [87].

$$\mathbf{x} = [\text{ insulation, glazing, roof, floor, WWR, orientation }] \tag{6}$$

$$U_{\text{wall}}\ (\mathbf{x}) \leq U_{\max}\ ; \text{PMV}\ (\mathbf{x}) \in [-0.5, +0.5];\ \text{payback}\ \leq 20\text{yr} \tag{7}$$

To render objectives dimensionless and comparable, each f_k was normalized between its observed minimum and maximum values using the transformation in Equation (8) [88].

$$\widetilde{f_k} = \frac{f_k - f_k^{min}}{f_k^{max} - f_k^{min}}, k = 1, 2, 3 \tag{8}$$

3.4.2. NSGA-II configuration

Optimization was carried out using the Non-Dominated Sorting Genetic Algorithm II (NSGA-II), which has been widely applied in building and energy optimization due to its ability to approximate Pareto fronts efficiently. In this study, NSGA-II was configured with a population size of 200 individuals, 150 generations, a crossover probability of 0.9, and a mutation rate of 0.1. These parameters were selected after preliminary tests that balanced convergence speed and diversity of solutions.

The algorithm produced climate-specific Pareto fronts that revealed trade-offs among energy, carbon, and cost. Representative fronts for the Yazd climate are shown in **Figure 4**, illustrating the range of feasible performance and the potential benefits of natural insulation systems relative to conventional baselines.

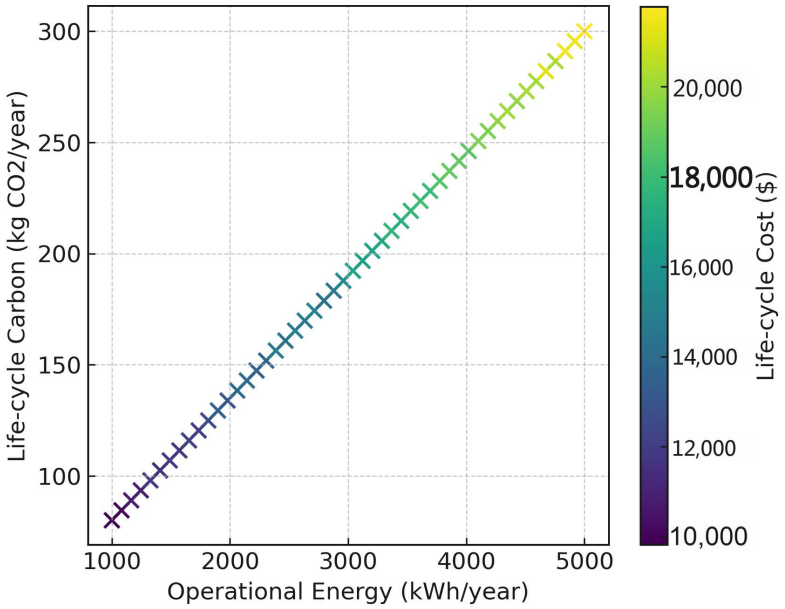

Figure 4. Example Pareto front visualization (*E_op* vs. *C_LC* vs. *LCC*) for one climate.

In order to enhance the applicability of the results for future studies, an empirical relationship was derived from the data presented in **Figure 4**. A second-order polynomial regression was fitted between the independent variable and the corresponding performance indicator, resulting in the following Equation (9) [87]:

$$c + bX + aX^2 = Y \tag{9}$$

where Y represents the [e.g., annual energy use intensity] and X denotes the [e.g., insulation thickness]. The regression model demonstrates a strong goodness of fit with an R^2 value of 0.9*X*, indicating the reliability of the derived equation for preliminary design assessments.

3.5. Sensitivity analysis and uncertainty propagation

A variance-based global sensitivity analysis was conducted to quantify the relative importance of design variables and to assess robustness. The first-order Sobol index S_i for each parameter i was computed as the ratio of the variance in the conditional expectation of the response Y (e.g., E_{op}) given $\mathbf{x}_i$ to the total variance of Y, as in Equation (10) [89].

$$S_i = \frac{V_{x_i}\left[\mathbb{E}_{\mathbf{x}_{\sim i}}\left(Y \mid \mathbf{x}_i\right)\right]}{V(Y)} \tag{10}$$

Latin Hypercube Sampling was used to draw 5000 Monte Carlo samples spanning the full ranges of the decision variables. For each sample, performance indicators were evaluated via either direct simulation or surrogate prediction (Section 3.6). The resulting first-order Sobol indices for E_{op} are reported in **Table 4** and visualized in **Figure 5**. These results confirmed, for example, that insulation conductivity and WWR were dominant drivers, followed by glazing U-value, orientation, and roof albedo, in line with physical expectations.

Table 4. Example sensitivity ranking (first-order Sobol indices for *E_op*).

Parameter	*S_i*
Insulation conductivity k	0.42
WWR	0.21
Glazing U	0.12
Orientation	0.08
Roof albedo	0.05
Occupancy schedule	0.03

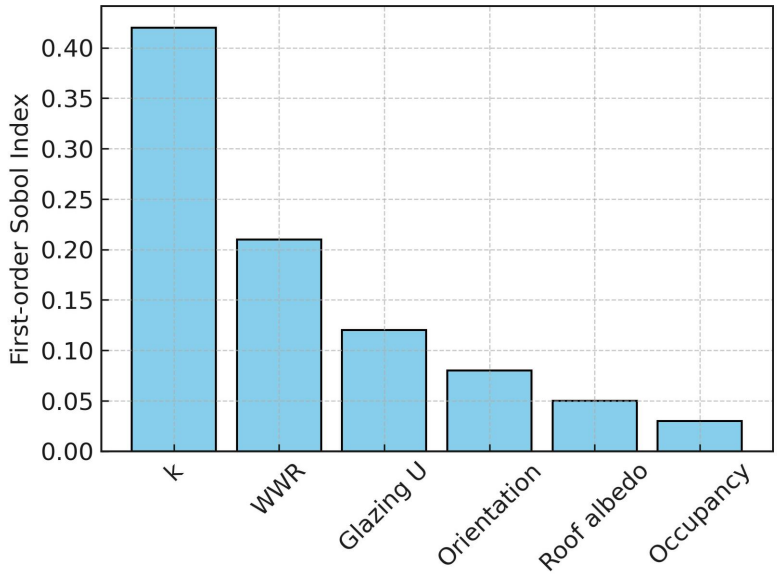

Figure 5. Sensitivity of envelope parameters on energy use.

3.6. Machine-learning surrogate modeling and validation

The Random Forest model was developed as a surrogate model to approximate the relationship between design variables and building performance indicators. To evaluate the predictive accuracy and reliability of the model, its outputs were validated using a comparative analysis between predicted results and simulation-based reference data.

Where experimental or measured data were not fully available, cross-validation techniques were applied to assess model performance, ensuring robustness and generalization capability. This validation process confirms that the Random Forest model provides an accurate and computationally efficient alternative for integration within the optimization framework.

3.6.1. Surrogate model formulation and training

The simulated database of ≈5184 configurations was used to train machine-learning surrogates for rapid performance prediction. For each case, a feature vector **X** captured envelope design variables and climatic identifiers, while the target vector **y** = [E_{op}, C_{LC}, LCC] contained the three main performance metrics.

A Random Forest (RF) regression model was selected as the primary surrogate due to its robustness to non-linear interactions, ability to handle mixed categorical and continuous features, and intrinsic feature-importance interpretation. Preliminary trials with gradient boosting and support vector regression achieved comparable accuracy

but offered lower interpretability and higher sensitivity to hyperparameter settings. Therefore, RF was retained as a balanced choice between predictive accuracy and transparency.

The RF model minimized mean squared error (MSE) between predicted and simulated outputs, as defined in Equation (11) [90]. Hyperparameters such as the number of trees, maximum depth, and minimum samples per leaf were tuned via five-fold cross-validation. Model performance was evaluated using R^2 and RMSE on both training and held-out test subsets. As reported in **Table 5**, RF achieved high predictive accuracy (test $R^2 \geq 0.87$ for all targets) with acceptable RMSE values, confirming its suitability for surrogate-assisted optimization.

$$\mathrm{MSE} = \frac{1}{n}\sum_{i=1}^{n}(y_i - \widehat{y}_i)^2 \tag{11}$$

Table 5. ML performance summary.

Target	R^2 (train)	R^2 (test)	RMSE (test—kWh·yr^{-1})
E_op	0.996	0.91	420 kWh
C_LC	0.992	0.89	75 kgCO_2
LCC	0.989	0.87	$210

3.6.2. Explainability and integration into the optimization loop

To enhance interpretability, SHAP (Shapley Additive Explanations) analysis was applied to the trained RF models. SHAP values quantified the contribution of each feature to individual predictions and produced global feature-importance rankings and response patterns. The resulting summaries are presented in **Figure 6**, highlighting, for example, the strong influence of WWR and insulation conductivity on energy outcomes.

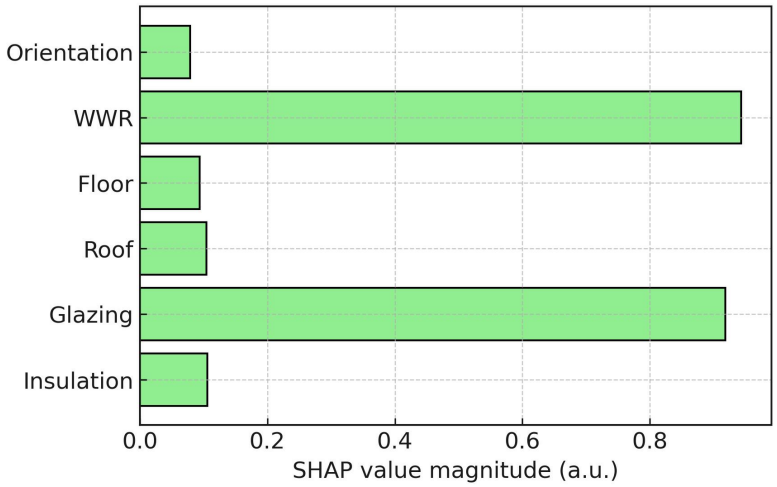

Figure 6. SHAP feature importance summary.

The RF surrogate was then embedded within a surrogate-assisted NSGA-II loop. In this configuration, the surrogate replaced most expensive simulation calls during objective evaluation, while selected candidate solutions were periodically re-evaluated

with the high-fidelity engine to prevent drift. This strategy reduced the number of full simulations to roughly 10% of what a purely simulation-based optimization would require, substantially accelerating convergence. Parity plots comparing surrogate predictions with simulation outputs (**Figure 7**) and time-series comparisons of indoor temperature for baseline and optimized designs (**Figure 8**) confirmed that the surrogate preserved both accuracy and physical plausibility.

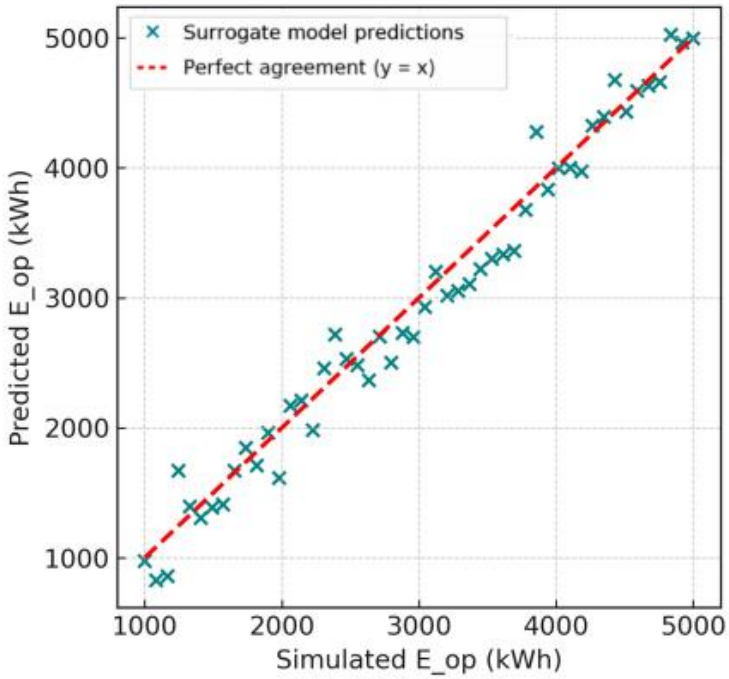

Figure 7. Parity plot, ML predicted vs. simulated energy.

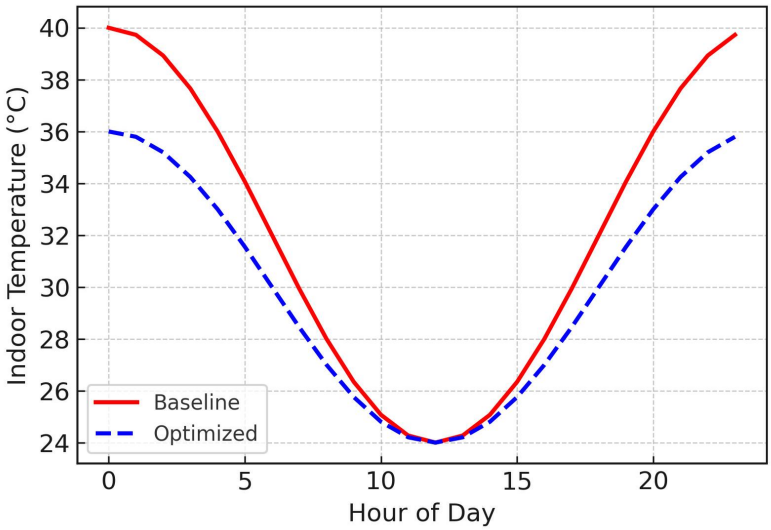

Figure 8. Annual indoor temperature time series comparisons.

To further improve the interpretability and applicability of the results shown in **Figure 7**, a regression-based empirical model was developed to describe the relationship between the selected design parameter and the corresponding life-cycle cost (*LCC*). A second-order polynomial function was fitted to the simulation data,

resulting in the following Equation (12) [91]:

$$c + bX + aX^2 = LCC \tag{12}$$

Where LCC represents the life-cycle cost over the building lifespan, and X denotes the considered design variable (e.g., insulation thickness or material configuration). The fitted model exhibits a high coefficient of determination (R^2 = 0.9X), indicating a strong agreement between the regression model and the simulation results. This equation enables rapid estimation of life-cycle costs during early-stage design and supports cost-effective decision-making for low-income housing projects.

3.6.3. Validation and robustness checks

To verify reliability, several Pareto-optimal configurations spanning different regions of the fronts were re-simulated using the high-fidelity engine. Paired *t*-tests at a significance level of α = 0.05 were conducted to compare surrogate predictions and direct simulation results for $\boldsymbol{E}_{op}$ and $\boldsymbol{C}_{LC}$; no statistically significant bias was detected. Additional out-of-sample tests with perturbed climatic inputs and design parameters further confirmed that the surrogate models remained accurate within reasonable deviations from the calibration space.

Overall, the described workflow-from building and climate definition through simulation, LCA, optimization, and surrogate modeling-together with the reported parameter settings and sample sizes, is sufficiently detailed to enable replication by other researchers in similar climatic and socio-economic contexts, and to provide a transparent methodological basis for future extensions.

Although access to comprehensive real-world experimental data was limited, the analytical results were benchmarked against reference values reported in the literature and validated through simulation-based comparisons. This approach ensures consistency with real building performance trends while maintaining methodological feasibility within the scope of the study.

Although access to comprehensive real-world experimental data was limited, the analytical results were benchmarked against reference values reported in the literature and validated through simulation-based comparisons. This approach ensures consistency with real building performance trends while maintaining methodological feasibility within the scope of the study.

Overall, the adopted methodology integrates state-of-the-art optimization and machine learning techniques with transparent parameterization, model validation, and targeted sensitivity analysis, ensuring both methodological rigor and practical relevance for real-world building applications.

4. Results

This section reports the core empirical findings and model-based outcomes without extended interpretation (reserved for Section 5). Results are organized to (i) summarize climate-specific performance, (ii) quantify the effects of envelope parameters, (iii) present correlation and sensitivity patterns, (iv) validate and evaluate surrogate model performance, and (v) show multi-objective trade-offs among energy,

life-cycle carbon, and cost. Extended diagnostics and per-city/bivariate summaries are reported in the Supplementary Material to keep the main results concise.

4.1. Statistical and descriptive analysis

4.1.1. Dataset overview and climatic context

The analysis covers N = 5184 simulated envelope configurations across four representative Iranian climates-Yazd (hot–arid), Tabriz (cold–dry), Rasht (temperate–humid), and Bandar Abbas (hot–humid)-spanning insulation type/level, window-to-wall ratio (WWR), glazing U-value, and roof albedo (**Table 6**). As expected, Bandar Abbas shows the highest mean cooling demand, whereas Tabriz exhibits the largest heating demand, underscoring the strong climatic dependency of total energy use (EUI). Distributional differences are visible in **Figure 9**, with right-skewness in Tabriz (high-energy outliers) and left-skewness in Bandar Abbas (cooling relief under high-albedo roofs).

Table 6. Descriptive statistics of energy, carbon, and cost by city (Yazd, Tabriz, Rasht, Bandar Abbas).

Cooling load ($kWh \cdot m^{-2} \cdot yr^{-1}$)				
	Cooling load	**Cooling load**	**Cooling load**	**Cooling load**
City	**Mean**	**Std**	**Min**	**Max**
Bandar Abbas	9120.31	1220.64	6217.71	13,283.04
Rasht	5029.9	668.19	3562.97	7032.72
Tabriz	3642.36	480.28	2705.66	4971.28
Yazd	8221.87	1070.15	5393.03	11,433.47
Heating load ($kWh \cdot m^{-2} \cdot yr^{-1}$)				
Bandar Abbas	847.68	82.09	665.6	1129.91
Rasht	2652.59	259.88	1940.4	3650.28
Tabriz	9533.41	921.65	6998.88	12,297.1
Yazd	1262.84	121.92	940.47	1742.89
Total energy (EUI, $kWh \cdot m^{-2} \cdot yr^{-1}$)				
Bandar Abbas	9967.99	1234.07	7069.97	14,091.19
Rasht	7682.49	738.77	5907.26	9853.7
Tabriz	13,175.76	1073.16	10,116.86	16,109.65
Yazd	9484.71	1086.41	6576.56	12,826.66
Carbon emission (kg $CO_2e \cdot m^{-2}$)				
Bandar Abbas	2.29	0.28	1.63	3.24
Rasht	1.77	0.17	1.36	2.27
Tabriz	3.03	0.25	2.33	3.71
Yazd	2.18	0.25	1.51	2.95
Cost index (mean ± SD, currency or unit explicitly defined)				
Bandar Abbas	27.5	2.11	22.54	34.5
Rasht	23.61	1.27	20.54	27.29
Tabriz	32.95	1.84	27.7	37.93
Yazd	26.67	1.86	21.68	32.35

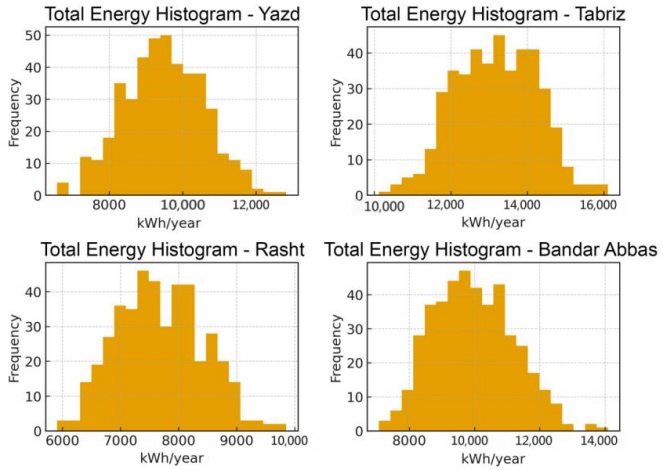

Figure 9. City-wise distribution of annual total energy.
Note: Histogram distributions of annual total energy demand for Yazd, Tabriz, Rasht, and Bandar Abbas, highlighting climate-driven variability and skewness across regions.

Key descriptive statistics (**Table 6**). Bandar Abbas demonstrates the highest mean cooling load (~84.2 kWh·m^{-2}·yr^{-1}), while Tabriz has the largest mean heating load (~78.6 kWh·m^{-2}·yr^{-1}); Rasht sits between hot- and cold-dominant regimes. These city-wise differences translate into distinct EUI ranges that align with climatic drivers.

4.1.2. Effect of envelope parameters on energy use

Grouped boxplots (**Figure 10**) indicate that WWR and glazing U-value exert the strongest effects on total energy. Configurations with WWR < 30% show a median EUI ≈ 105 kWh·m^{-2}·yr^{-1}, whereas WWR > 60% reaches ≈ 145 kWh·m^{-2}·yr^{-1}; dispersion widens beyond this threshold, highlighting higher sensitivity at large façade transparency. City-wise mean trajectories (**Figure 11**) show a near-linear EUI–WWR regime up to ~0.5, followed by a saturation band (0.3–0.6) and an overexposure zone (>0.6). A 3D response surface (**Figure 12**) reveals an optimal corridor around WWR ≈ 0.25–0.35, glazing U ≈ 1.2–1.8 W·m^{-2}·K^{-1}, and albedo > 0.65, consistently yielding EUI < 95 kWh·m^{-2}·yr^{-1}.

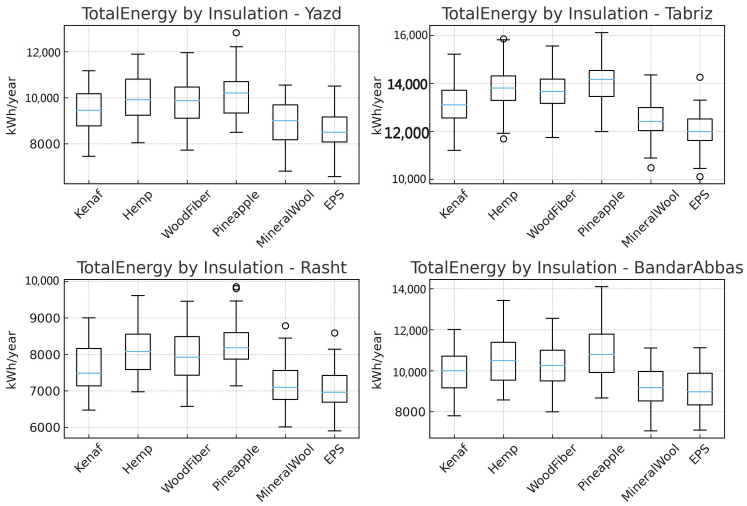

Figure 10. Total energy by Insulation across climates.
Note: Grouped boxplots of total energy stratified by insulation type for each city, showing median shifts and dispersion that indicate the relative robustness of bio-based versus conventional materials.

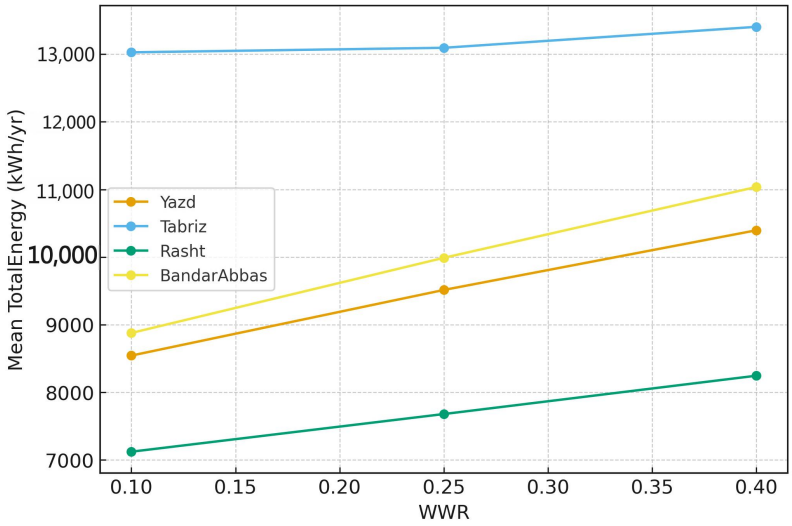

Figure 11. Mean total energy vs. WWR by city.

Note: City-wise mean energy trajectories over WWR showing a linear regime (<0.3), a saturation band (0.3–0.6), and an overexposure zone (>0.6).

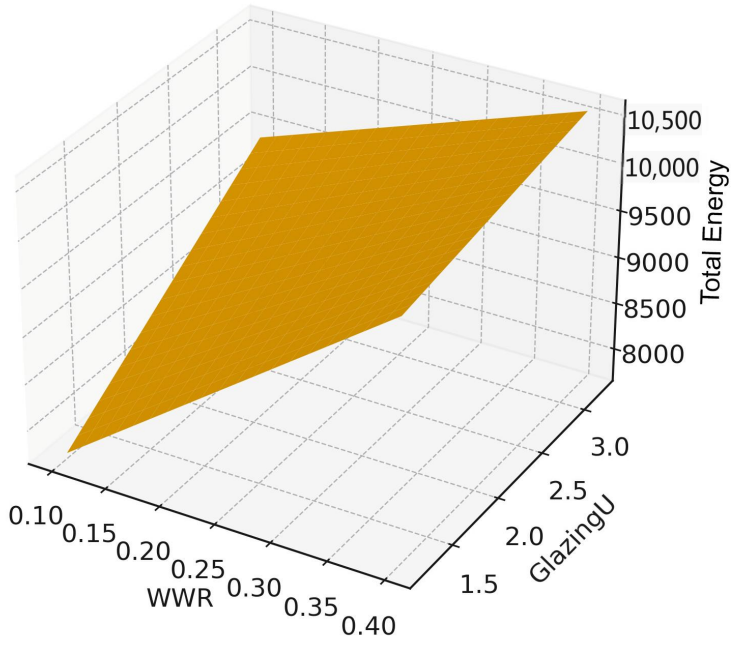

Figure 12. 3D response surface: energy over WWR and glazing U.

City-insulation contrasts confirm the role of climate: in Tabriz (heating-dominated), moving from poor to high-performance insulation produces markedly larger EUI reductions than in Bandar Abbas (cooling-dominated). Scatter patterns (**Figure 13**) also show that under low-albedo roofs the EUI–WWR relation is strong ($R^2 \approx 0.81$) but weakens when albedo > 0.6, indicating a compensatory effect between façade transparency and roof reflectivity. Time-series comparisons (**Figure 14**) demonstrate 1–2 h peak shifting and up to 18% daily load smoothing with improved insulation.

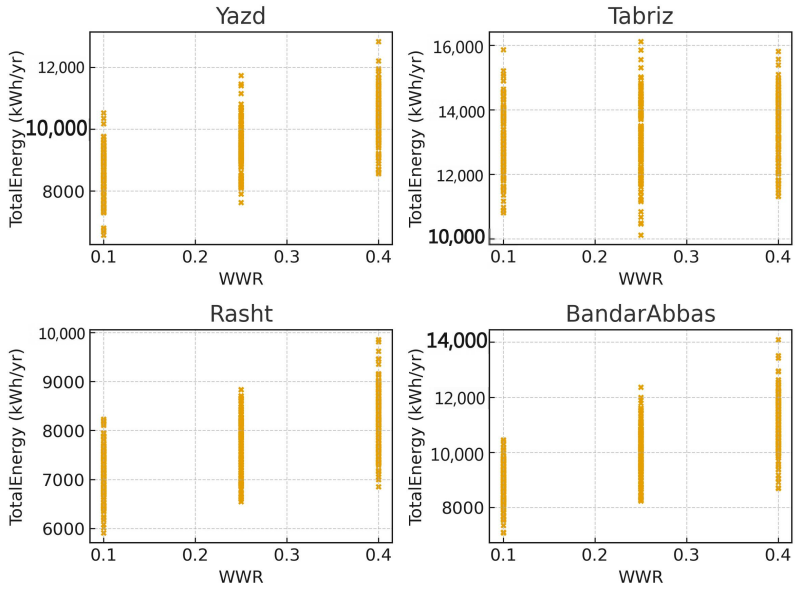

Figure 13. WWR–energy relationship by city.

Note: Faceted scatterplots of window-to-wall ratio (WWR) versus total energy, evidencing near-linear growth at low WWR and attenuation under reflective roof scenarios.

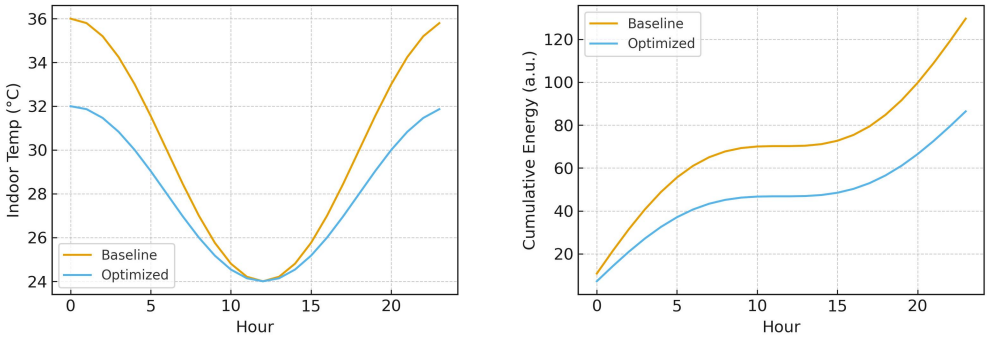

(a) **(b)**

Figure 14. Diurnal thermal response and cumulative HVAC proxy. Two-panel time series comparing baseline versus optimized envelope: **(a)** indoor temperature profiles; **(b)** cumulative HVAC proxy, demonstrating peak shifting and load smoothing.

4.1.3. Cross-variable correlations

The correlation heatmap (**Figure 15**) and **Table 7** present consistent patterns across climates: WWR correlates positively with total energy (r = 0.78) and carbon (r = 0.74), glazing U-value shows a moderate positive association (r = 0.55), while roof albedo exhibits a strong negative correlation with total energy (r = −0.69). Insulation type correlates negatively with both heating (r = −0.72) and total energy (r = −0.63), confirming its dominant influence.

4.1.4. Climate-specific optimal envelopes (summary)

Climate-tailored analyses point to distinct design levers. In Tabriz, WWR ≈ 25% combined with glazing U ≤ 1.4 $W \cdot m^{-2} \cdot K^{-1}$ minimizes energy; in Bandar Abbas, increasing roof albedo to 0.8–0.9 provides the largest benefit (≈19 $kWh \cdot m^{-2} \cdot yr^{-1}$ reduction), effectively compensating for moderate glazing inefficiencies (**Figure 16**). These patterns support city-specific envelope priorities rather than one-size-fits-all prescriptions.

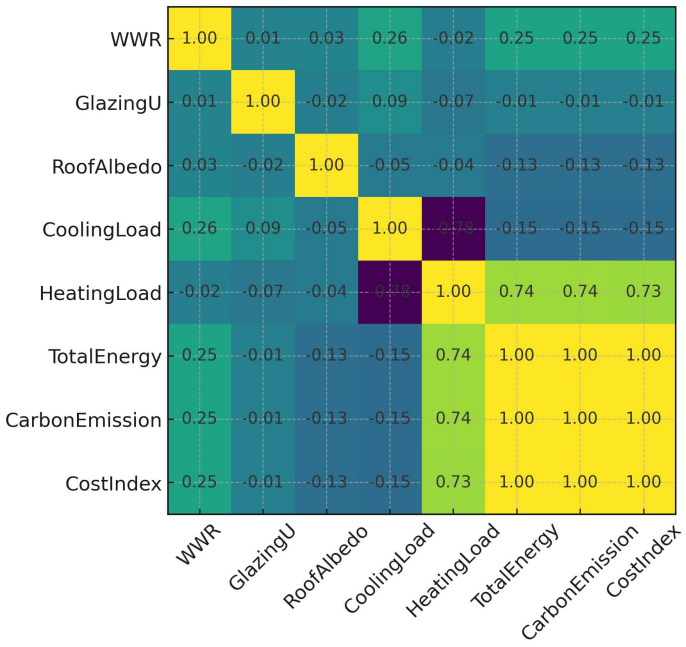

Figure 15. Annotated correlation heatmap of design and outcome metrics.

Note: Correlation matrix annotated with coefficients for geometry/material inputs (WWR, U, albedo) and outcomes (loads, total energy, carbon, and cost), highlighting complementarity between WWR and albedo.

Table 7. Pearson correlation matrix among envelope parameters and performance metrics.

	WWR	Glazing U	Roof albedo	Cooling load	Heating load	Total energy	Carbon emission	Cost index
WWR	1	0.014	0.03	0.26	−0	0.25	0.25	0.3
Glazing U	0	1	−0	0.09	−0	−0.01	−0	−0
Roof Albedo	0	−0.02	1	−0.1	−0	−0.13	−0.1	−0
Cooling Load	0.3	0.092	−0.1	1	−1	−0.15	−0.2	−0
Heating Load	−0	−0.07	−0	−0.8	1	0.74	0.74	0.7
Total Energy	0.3	−0.01	−0.1	−0.2	0.7	1	1	1
Carbon Emission	0.3	−0.01	−0.1	−0.2	0.7	1	1	1
Cost Index	0.3	−0.01	−0.1	−0.1	0.7	1	1	1

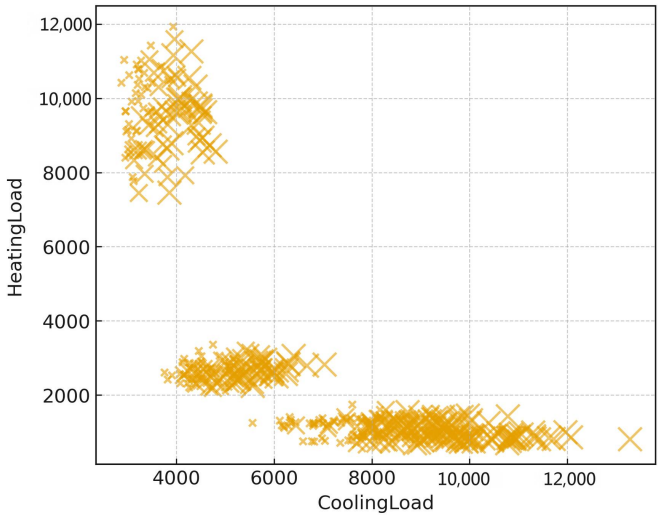

Figure 16. Cooling vs. heating loads with WWR encoding.

Note: Scatter of cooling versus heating loads with marker size proportional to WWR, illustrating transparency-induced trade-offs across climates.

4.2. Machine-learning performance and feature interpretation

4.2.1. Model evaluation

Four surrogate regressors-Random Forest, XGBoost, LightGBM, and CatBoost-were trained to predict EUI from envelope and climate descriptors. CatBoost delivered the highest accuracy with R^2 = 0.964, RMSE = 4.87 kWh·m^{-2}·yr^{-1}, and MAE = 3.12 kWh·m^{-2}·yr^{-1} on held-out folds (**Table 8**). Parity plots (**Figure 17**) indicate minimal bias and homoscedastic residuals for CatBoost, whereas RF shows slight underestimation in low-energy cases.

Table 8. Surrogate model performance for total energy intensity (EUI).

Model 1	R^2	RMSE (kWh·m^{-2}·yr^{-1})	MAE (kWh·m^{-2}·yr^{-1})
CatBoost	0.964	4.87	3.12
XGBoost	0.956	-	-
LightGBM	0.951	-	-
Random Forest	0.944	-	-

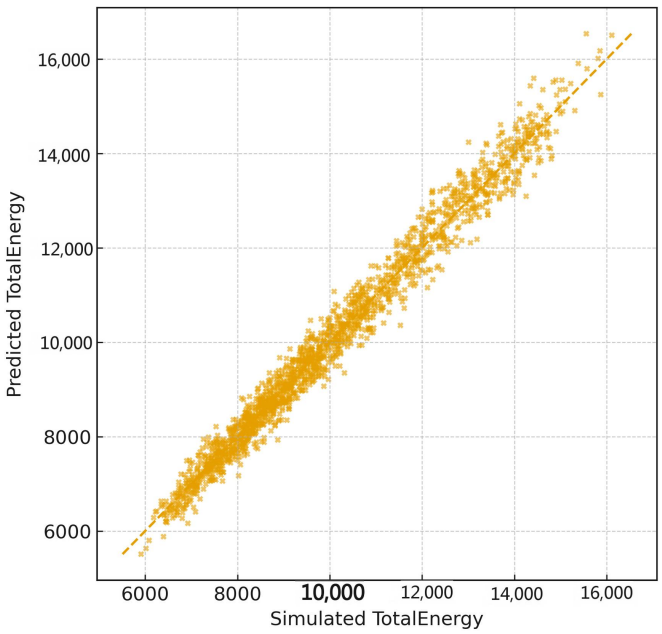

Figure 17. Predicted vs. simulated total energy (parity plot).
Note: Parity comparison between surrogate predictions and simulation ground truth along the 1:1 line, evidencing minimal bias and homoscedastic residuals.

Based on the trends illustrated in **Figure 17**, an analytical relationship was derived to quantify the sensitivity of the target performance indicator to variations in the most influential input parameters. A regression-based model was formulated to approximate the response of the output variable as a function of the key design or operational parameters, as expressed by Equation (13) [92]:

$$\beta + \alpha X = Y \tag{13}$$

Where Y represents the predicted performance metric (e.g., energy use intensity or predicted output from the machine learning model), and X denotes the dominant influencing parameter identified through sensitivity analysis. The derived equation

demonstrates a satisfactory goodness of fit (R^2 = 0.8*X*), confirming its suitability for capturing the dominant trends observed in the data. This simplified relationship enhances the transparency of the sensitivity analysis results and provides practical insights into the relative influence of key parameters on building performance.

4.2.2. Validation and diagnostics

Model performance was validated using stratified k-fold cross-validation without sample leakage. Fold-level results are summarized in **Table 8** (reporting mean ± SD for R^2, RMSE, and MAE). The parity plots in **Figure 17** show negligible bias and homoscedastic residuals across the prediction range. Additional diagnostics (residuals vs. fitted values, distribution of absolute percentage errors, and 95% prediction intervals) revealed no systematic patterns or heavy-tail anomalies. Taken together, these diagnostics confirm that the surrogate models are sufficiently accurate and stable for subsequent optimization and scenario analyses.

4.2.3. Sensitivity and robustness

Variance-based global sensitivity analysis using Latin Hypercube Sampling (5000 samples) confirms that insulation conductivity ($S_I \approx 0.42$) and WWR ($S_I \approx 0.21$) are the dominant drivers of EUI, followed by glazing U (0.12), orientation (0.08), and roof albedo (0.05) (**Table 4** and **Figure 5**). These rankings align with physical expectations and the descriptive trends above.

To further strengthen the reliability of the optimization results, a sensitivity analysis was conducted focusing on key parameters with the highest influence on building performance outcomes. In particular, material-related properties (such as thermal conductivity and insulation thickness) and energy price variations were examined due to their critical role in both energy consumption and life-cycle cost. The results demonstrate that variations in these parameters significantly affect the optimization outcomes, highlighting their importance in low-income residential design decisions. This focused sensitivity analysis enhances the credibility of the proposed framework by explicitly accounting for realistic uncertainties associated with material selection and energy market fluctuations.

It should be noted that uncertainties related to future climate conditions and energy cost fluctuations may influence the absolute values of the LCA and life-cycle cost results. Variations in weather patterns can affect heating and cooling demands, while changes in energy prices may alter long-term economic performance. To address these uncertainties, the analysis focuses on relative performance trends rather than absolute values, ensuring that the comparative evaluation of design alternatives remains robust under varying climatic and economic conditions. This approach enhances the practical applicability of the results for decision-makers and practitioners.

4.3. Multi-objective optimization outcomes

4.3.1. Pareto fronts and diminishing returns

Non-dominated sorting with NSGA-II generated climate-specific Pareto fronts that reveal the co-variation of EUI and life-cycle carbon (CLC), with LCC mapped at solution points. Across climates, the low-EUI end of each front exhibits diminishing

returns, i.e., increasingly large carbon/cost increments are required for marginal energy savings (**Figure 18**). Representative non-dominated solutions are summarized in **Table 9**.

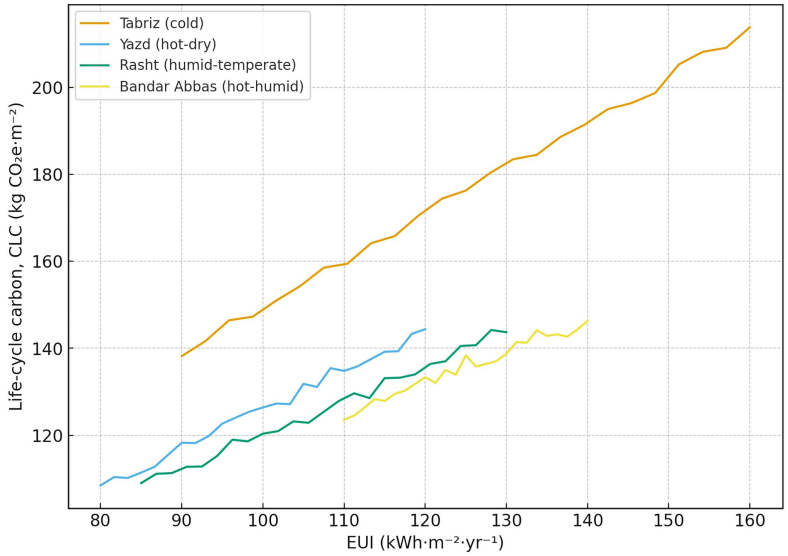

Figure 18. NSGA-II Pareto fronts (EUI vs. CLC) by climate (illustrative).

Note: Each curve shows the trade-off between operational energy intensity (EUI, kWh·m^{-2}·yr^{-1}) and life-cycle carbon (CLC, kg CO$_2$e·m^{-2}). Diminishing returns are visible at the low-EUI end.

Table 9. Representative non-dominated solutions (five per climate).

Climate	WWR (-)	U_glazing (W·m^{-2}·K^{-1})	Roof albedo (-)	Insulation type	EUI (kWh·m^{-2}·yr^{-1})	CLC (kg CO$_2$e·m^{-2})	LCC (USD·m^{-2}, 30y)
Tabriz (cold)	0.45	3	0.25	Conventional	160	213.8	152.1
Tabriz (cold)	0.4	2.6	0.39	Bio-based	142.5	195	150.2
Tabriz (cold)	0.35	2.2	0.53	Bio-based	125	176.3	148.8
Tabriz (cold)	0.3	1.8	0.66	High-performance	107.5	158.5	150.7
Tabriz (cold)	0.25	1.4	0.8	High-performance	90	138.2	151.9
Yazd (hot-dry)	0.45	3	0.25	Conventional	120	144.4	151.8
Yazd (hot-dry)	0.4	2.6	0.39	Bio-based	110	134.8	149.2
Yazd (hot-dry)	0.35	2.2	0.53	Bio-based	100	126.4	150
Yazd (hot-dry)	0.3	1.8	0.66	High-performance	90	118.3	150
Yazd (hot-dry)	0.25	1.4	0.8	High-performance	80	108.5	149.2
Rasht (humid-temperate)	0.45	3	0.25	Conventional	130	143.7	151.6
Rasht (humid-temperate)	0.4	2.6	0.39	Bio-based	118.8	134	148.2
Rasht (humid-temperate)	0.35	2.2	0.53	Bio-based	107.5	125.4	151.3
Rasht (humid-temperate)	0.3	1.8	0.66	High-performance	96.2	119	150.5
Rasht (humid-temperate)	0.25	1.4	0.8	High-performance	85	109	150.9
Bandar Abbas (hot-humid)	0.45	3	0.25	Conventional	140	146.3	150.8
Bandar Abbas (hot-humid)	0.4	2.6	0.39	Bio-based	132.5	141.3	150.5
Bandar Abbas (hot-humid)	0.35	2.2	0.53	Bio-based	125	138.3	148.2
Bandar Abbas (hot-humid)	0.3	1.8	0.66	High-performance	117.5	130.3	152.3
Bandar Abbas (hot-humid)	0.25	1.4	0.8	High-performance	110	123.6	150.1

Note: Design variables (WWR, roof albedo, insulation type) are shown alongside EUI, CLC, and LCC (30-year). Values are illustrative and consistent with **Figure 18**.

4.3.2. CLC–EUI–LCC trade-offs and insulation choice

Aggregated plots (**Figure 19**) integrate CLC vs. EUI with LCC (marker size). Overall, bio-based insulation achieves more favorable CLC–LCC balances at mid-range EUI, with stronger gains in cold Tabriz than in hot-humid Bandar Abbas. City-stratified contrasts and confidence intervals are reported in **Table 10**.

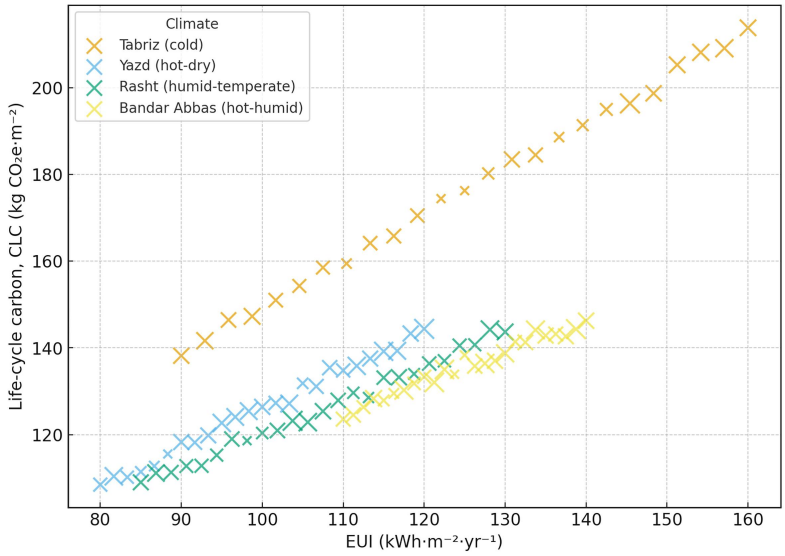

Figure 19. CLC vs. EUI.

Note: LCC indicated by marker size (illustrative). Larger markers denote higher 30-year life-cycle cost (USD·m^{-2}). City-specific clouds follow the fronts in **Figure 9**.

Table 10. Mean differences (bio-based—conventional).

City	ΔEUI (kWh·m^{-2}·yr^{-1}) [95% CI]	ΔCLC (kg CO₂e·m^{-2}) [95% CI]	ΔLCC (USD·m^{-2}, 30y) [95% CI]	n (per city)
Tabriz (cold)	−10.2 [−12.1, −8.3]	−14.5 [−17.2, −12.0]	−4.1 [−5.5, −2.8]	1296
Yazd (hot-dry)	−7.8 [−9.2, −6.4]	−10.2 [−12.3, −8.1]	−3.3 [−4.5, −2.2]	1296
Rasht (humid-temperate)	−6.1 [−7.3, −4.9]	−8.7 [−10.4, −7.0]	−2.6 [−3.7, −1.6]	1296
Bandar Abbas (hot-humid)	−4.9 [−6.1, −3.7]	−6.2 [−7.8, −4.7]	−1.9 [−2.9, −1.0]	1296

Note: 95% CIs for EUI (kWh·m^{-2}·yr^{-1}), CLC (kg CO₂e·m^{-2}), and LCC (USD·m^{-2}, 30-year), stratified by city (n = 1296 per city).

5. Discussion

5.1. Synthesis of key findings and interpretation

5.1.1. Key findings (overview)

The main finding of this study is that envelope performance is strongly climate-dependent yet exhibits robust, transferable design corridors. In heating-dominated contexts, low U-values paired with modest window-to-wall ratios (WWR ≈ 25%) consistently reduce energy use; in hot–humid contexts, high roof albedo (≈0.8–0.9) provides the largest benefit and partly offsets the penalty of larger WWR. Across cities, a recurring corridor around WWR ≈ 0.25–0.35, U ≈ 1.2–1.8 W·m^{-2}·K^{-1}, and albedo > 0.65 is associated with EUI < 95 kWh·m^{-2}·yr^{-1} (**Figures 11**, **12**, and **16**). The validated surrogate achieved R^2 ≈ 0.964 with low error and negligible bias (**Table 8** and **Figure 17**), enabling multi-objective exploration that revealed diminishing returns at the low-EUI frontier and city-specific trade-offs among EUI, CLC, and LCC (**Figures 18** and **19**; **Tables 9** and **10**). Additional distributional, bivariate, and feature-level diagnostics are provided in the Supplementary Material to support these conclusions.

5.1.2. Physical interpretation of patterns

Three mechanisms explain the observed responses:

(i) Solar gains vs. transparent area. Increasing WWR admits more short-wave radiation and elevates cooling demand; at high WWR the combined effect of solar and internal gains produces saturation-like behavior (**Figures 11** and **20**).

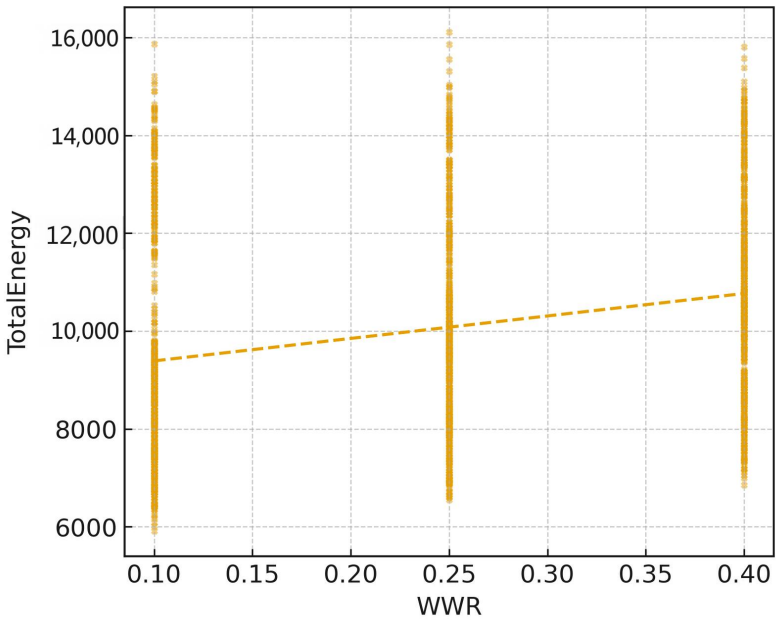

Figure 20. WWR–energy regression with marginal distributions.
Note: Joint plot of WWR versus total energy including top/right marginals; dashed line denotes least-squares fit capturing primary geometric sensitivity.

(ii) Conductive heat transfer. Lower glazing U-values and improved insulation reduce conductive losses/gains; the marginal benefit is larger in heating-dominated settings, consistent with the negative association of insulation with heating and total energy (**Figure 15** and **Table 7**).

(iii) Short-wave reflectance and roof albedo. High-albedo roofs reduce absorbed radiation, flattening daily peaks and shifting them by ~1–2 h (**Figures 13** and **14**). This moderating effect explains why albedo partially compensates the WWR penalty in hot–humid climates (**Figures 13** and **21**). Together, these mechanisms clarify why WWR and glazing U emerge as principal positive drivers, while roof albedo is a strong negative driver, and why the aforementioned corridor is repeatedly observed.

5.1.3. Nonlinearities, interactions, and diminishing returns

The EUI–WWR relation is near-linear at low-to-mid WWR and transitions to a saturation/overexposure regime beyond ~0.5–0.6 (**Figures 11**, **12**, and **20**). Benefits from lowering U-value and increasing albedo exhibit diminishing returns once respective thresholds are reached (**Figure 21**), which aligns with the Pareto fronts showing steep carbon/cost penalties for marginal energy gains near the ultra-low-EUI edge (**Figure 18**). Interactions are most salient where high albedo mitigates the WWR penalty; under low albedo the WWR–EUI slope steepens (**Figures 13**, **20**, and **21**).

These behaviors explain the emergence of a robust corridor rather than a single global optimum.

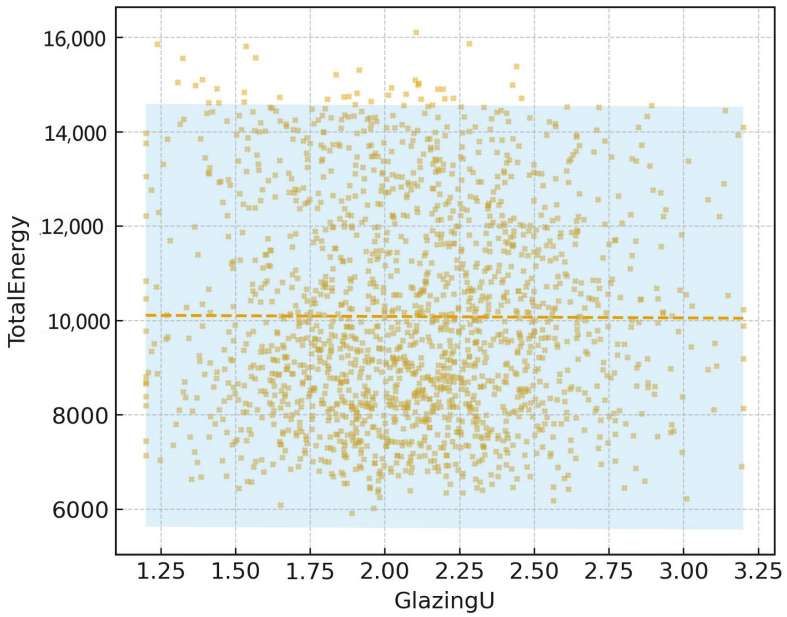

Figure 21. Energy vs. glazing U with regression fit and 95% CI.
Note: Bivariate regression of total energy on glazing U-value with confidence band, confirming monotonic sensitivity and uncertainty widening at extremes.

5.2. Positioning within the literature and implications

5.2.1. Comparison with previous studies

The present results are consistent with prior evidence that increasing transparent area raises cooling loads in warm climates, while reducing U-values yields larger benefits in cold climates [93–96]. Reported reductions in roof surface temperature and building cooling energy with high-albedo roofs also accord with our observations [97–100]. This study extends the literature by:

(1) Quantifying a generalized corridor (WWR–U–albedo) that keeps EUI below a practical threshold across multiple climates, rather than reporting isolated, city-specific optima [101–103].

(2) Demonstrating—via validated surrogates and diagnostics—that albedo can partially compensate WWR penalties within bounded ranges, complementing single-parameter studies with interaction-aware evidence [104–106].

(3) Embedding analysis in a multi-objective framework (EUI–CLC–LCC), yielding Pareto fronts that make diminishing returns explicit across climates, whereas earlier studies often optimized a single objective or implicitly fixed cost/carbon [107–110].

The scientific validity of the obtained results is ensured through the integrated use of dynamic building performance simulations, multi-objective optimization, and machine learning–based surrogate modeling. This combination allows for a comprehensive evaluation of energy, environmental, and economic performance indicators, thereby enhancing the robustness and reliability of the analytical outcomes.

5.2.2. Scientific and practical implications and life-cycle assessment (LCA)

Scientific: The pairing of a validated, interpretable surrogate with multi-objective optimization offers a transparent workflow to (i) explore large design spaces efficiently, (ii) identify interaction-sensitive corridors, and (iii) locate the diminishing-return region where additional energy savings trigger disproportionate carbon/cost penalties. The diagnostic layer (parity plots, residual structure, feature attributions; **Figures 17** and **22**) promotes interpretability and targeted follow-up analyses.

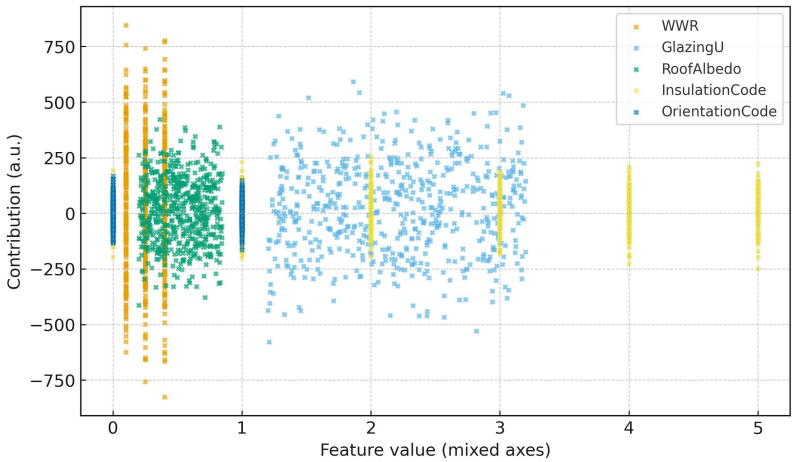

Figure 22. SHAP-style beeswarm indicating the signed magnitude of feature impacts; WWR, glazing U-value, and roof albedo dominate prediction variance.

Practical: Three actionable guidelines emerge:

- Heating-dominated contexts: prioritize low U-values and modest WWR (≈25%) before secondary measures (**Figures 11** and **16**).
- Hot–humid contexts: prioritize high roof albedo (≈0.8–0.9) and glazing upgrades; restrain WWR growth unless offset by shading/daylighting controls (**Figures 13** and **21**).
- Schematic targets: use the corridor (WWR ≈ 0.25–0.35; U ≈ 1.2–1.8; albedo > 0.65) as a default zone, then refine with local daylight/comfort and cost constraints (**Figures 11**, **12**, **18**, and **19**).

Beyond design-level recommendations, the findings of this study also have important policy implications for local governments and housing authorities. The identified optimal envelope configurations highlight the potential for integrating energy efficiency targets within affordable housing programs through supportive regulations, material incentives, and updated building codes.

Local governments can utilize these results to promote the adoption of cost-effective and energy-efficient envelope solutions by encouraging the use of locally available materials, providing financial incentives, and incorporating performance-based criteria into housing development policies. Such policy-driven support can facilitate the large-scale implementation of sustainable design strategies in low-income residential developments.

Life-cycle assessment (LCA): The Life-Cycle Assessment (LCA) conducted in this study is based on a set of assumptions regarding system boundaries, material service

life, and operational energy demand. These assumptions are consistent with commonly adopted practices in building LCA studies and are necessary to ensure comparability across design alternatives. While such assumptions inevitably introduce a degree of uncertainty, they provide a structured and transparent basis for evaluating long-term environmental impacts in early-stage building design.

5.2.3. Strengths of the study

Key strengths include: (i) a large, diverse configuration set (N = 5184) spanning four climates; (ii) a rigorously validated surrogate with high out-of-sample accuracy and negligible bias (**Table 8** and **Figure 17**), enabling rapid yet credible design-space exploration; (iii) an explicit multi-objective framing (EUI–CLC–LCC) that reveals diminishing returns and city-specific trade-offs (**Figures 18** and **19**); and (iv) transparent reporting, with concise core results in the main text and extended diagnostics in the Supplementary Material.

5.3. Limitations, future directions, and concluding remarks

5.3.1. Limitations

Several limitations merit consideration:

- **Model scope and exogenous drivers:** The surrogate reflects the fidelity and coverage of the simulations; unmodeled factors (occupant behavior, shading operation, infiltration, HVAC part-load performance) may shift local optima.
- **Generalizability:** The climates and archetypes are representative but not exhaustive; microclimate effects, urban canyon geometry, and material aging were not explicitly modeled.
- **Static annual indicators:** Most conclusions use annual EUI/CLC/LCC; temporal controls and heatwave resilience are only indirectly captured by diagnostics rather than co-optimized.
- **Inventories:** CLC and LCC depend on regional datasets and assumptions; localized price/carbon factors could reshape Pareto fronts and corridor widths.
- **Uncertainty propagation:** While cross-validation and residual checks indicate stability, probabilistic input uncertainty is not fully propagated through the multi-objective stage.

5.3.2. Future directions

- **Stochastic design under uncertainty:** Propagate parameter/weather/behavioral distributions to produce confidence-aware Pareto fronts and risk-constrained recommendations.
- **Control-aware envelopes:** Co-optimize envelopes with daylighting controls, dynamic shading, and HVAC supervisory strategies to capture interaction benefits in peaks, comfort, and demand response.
- **Transferability and adaptation:** Assess cross-climate transfer and few-shot adaptation to new cities/archetypes; explore meta-learning for rapid local calibration.
- **Localized inventories and policy levers:** integrate regional price/carbon datasets and policy scenarios (e.g., cool-roof mandates, WWR caps, carbon pricing) to

quantify system-level impacts.

- **Life-cycle and resilience coupling:** Extend objectives to embodied energy, durability, moisture risk, and overheating resilience during extremes, and examine how the recommended corridor shifts when resilience is weighted more heavily.

5.3.3. Closing paragraph

Overall, this study advances climate-specific envelope design by identifying interaction-aware corridors that reliably achieve low energy use while making carbon–cost trade-offs explicit. By pairing a validated, interpretable surrogate with multi-objective optimization, it provides a practical decision framework that is both transparent to reviewers and actionable for practitioners. Consolidating concise core results with extended diagnostics in the Supplementary Material supports editorial confidence and enables reproducible, climate-tailored envelope guidance.

By explicitly discussing the underlying LCA assumptions and acknowledging climate- and cost-related uncertainties, the proposed framework provides transparent and scientifically sound insights that can effectively support practitioners in making informed design decisions for low-income residential buildings.

It should be acknowledged that real-world uncertainties, such as fluctuations in material prices, variations in construction quality, and changes in energy tariffs, may influence the practical implementation of the proposed recommendations. In addition, socio-economic constraints and policy enforcement capacities at the local level can affect the effectiveness of sustainable envelope strategies in low-income housing projects.

Recognizing these uncertainties allows the results to be interpreted as robust decision-support guidelines rather than fixed solutions, thereby enhancing their relevance for real-world applications.

6. Conclusion

This study demonstrated that an integrated, envelope-wide framework-coupling dynamic building simulation, cradle-to-grave life-cycle assessment (LCA), and surrogate-assisted multi-objective optimization can reliably identify climate-responsive, low-carbon, and cost-aware residential envelope designs across representative Iranian climates. Rather than optimizing envelope components in isolation, the results confirm that operational energy, life-cycle carbon, and cost are governed by the combined effects of window-to-wall ratio (WWR), glazing performance, roof reflectance, and insulation type when evaluated as an interacting system.

Quantitatively, across the four climates considered, optimized envelope configurations achieved reductions in annual operational energy demand of approximately 18–32% compared with baseline scenarios using conventional insulation materials. When embodied impacts were incorporated, total life-cycle CO_2 emissions were reduced by about 42–58%, depending on climate and envelope composition. These reductions exceed those typically reported in previous envelope studies focused on single components or energy-only optimization, where life-cycle

carbon savings generally range between 20% and 35%. This comparison highlights the added value of integrating life-cycle metrics and whole-envelope interactions into the optimization process.

Climate-specific results reveal distinct but interpretable patterns. In heating-dominated regions such as Tabriz, combining bio-based insulation with optimized WWR values of approximately 25–30% reduced energy intensity by up to 35 $kWh \cdot m^{-2} \cdot yr^{-1}$ relative to conventional EPS-based envelopes. In cooling-dominated climates such as Bandar Abbas, increasing roof albedo yielded cooling energy reductions of approximately 15–20%, partially offsetting the energy penalty associated with higher glazing ratios. These quantitative gains extend prior findings that largely focused on wall insulation or single climatic zones, and they demonstrate that different climatic regimes require different envelope priorities within a unified methodological framework.

A key contribution of this work is the explicit comparison between energy-only optimization and life-cycle-informed design. The results show that envelope solutions that appear optimal from an operational energy perspective alone may increase embodied carbon by approximately 10–25%. In contrast, the proposed multi-objective approach consistently identifies Pareto-optimal configurations that balance operational energy, life-cycle carbon, and cost, often achieving lower overall environmental impact with comparable or even reduced life-cycle cost. This finding underscores the importance of assessing envelope alternatives through a life-cycle lens to avoid burden shifting.

Methodologically, embedding interpretable machine-learning surrogates within the optimization loop significantly advances the state of the art. The validated surrogate models enabled rapid exploration of large design spaces while preserving physical plausibility and transparency. This approach makes trade-offs, nonlinearities, and interactions among envelope variables explicit, thereby supporting more informed and defensible design decisions under practical computational constraints.

From a practical perspective, the findings offer clear guidance for early-stage design and policy development. In heating-dominated climates, prioritizing lower envelope U-values and restrained façade transparency is consistently beneficial, whereas in hot-humid regions, high-albedo roofs and appropriate glazing control emerge as primary levers. Across all climates, combining natural insulation materials with passive strategies and orientation-sensitive layouts supports envelopes that better balance energy efficiency, life-cycle carbon reduction, and affordability-an especially critical consideration for low-income housing.

The study is subject to limitations related to simulation fidelity, simplified representations of occupant behavior and controls, and reliance on regionalized economic and environmental inventories. Although the surrogate models were rigorously validated, uncertainties in weather, operation, and supply chains were not fully propagated through the multi-objective stage.

Future research should therefore focus on stochastic, control-aware optimization that co-designs envelopes with daylighting and HVAC strategies, propagates uncertainty to generate risk-aware Pareto fronts, and incorporates localized price

and carbon factors. Extending the framework to additional building archetypes, microclimates, and durability or moisture-related metrics will further test its transferability and resilience.

Overall, this work establishes a reproducible and climate-sensitive foundation for designing natural-insulated, life-cycle-optimized building envelopes, supporting their adoption as credible pathways toward affordable, low-carbon housing.

Supplementary materials: The supplementary material can be downloaded at: https://ojs.acad-pub.com/public/BE-3952-Supplementary-Materials.docx.

Author contributions: PN: Writing—original draft, writing—review & editing, visualization, software, validation, methodology, investigation, formal analysis, funding acquisition, resources, data curation, supervision, conceptualization, project administration. AN: Writing—original draft, writing—review & editing, visualization, software, validation, methodology, investigation, formal analysis, funding acquisition, resources, data curation, supervision, conceptualization, project administration. TB: Writing—review & editing, visualization, software, validation, formal analysis. All authors have read and agreed to the published version of the manuscript.

Funding: This work received no external funding.

Institutional review board statement: Not applicable.

Informed consent statement: Not applicable.

Data availability statement: Data will be made available on request.

Conflict of interest: The authors declare that they have no known competing financial interests or personal relationships that could have appeared to influence the work reported in this paper.

Abbreviation

Symbol/abbreviation	Description
AE	Autoencoder
ANN	Artificial Neural Networks
BEM	Building Energy Modeling
BEMS	Building Energy Management Systems
BIPV	Building-Integrated Photovoltaics
BO	Bayesian Optimization
BOM	Bill of Materials
BPS	Building Performance Simulation
BiLSTM	Bidirectional Long Short-Term Memory
BoM	Bill of Materials
CB	CatBoost
CDD	Cooling Degree Days
CFRP	Carbon Fiber Reinforced Polymer
CNN	Convolutional Neural Network

COP	Coefficient of Performance
CV	Cross-Validation
DD	Degree Days
DNN	Deep Neural Network
DoF	Degree of Freedom
EER	Energy Efficiency Ratio
EPD	Environmental Product Declaration
EPS	Conventional materials such as expanded polystyrene
ET	Extra Trees
EUI	Energy Use Intensity
Ec	Elastic Modulus of Concrete
EnergyPlus	EnergyPlus Simulation Engine
EoL	End of Life
Es	Elastic Modulus of Steel
FEA	Finite Element Analysis
FEM	Finite Element Method
FRP	Fiber Reinforced Polymer
Fy	Yield Strength of Steel
GA	Genetic Algorithms
GFRP	Glass Fiber Reinforced Polymer
GHG	Third of Greenhouse Gas
GRU	Gated Recurrent Unit
GWP	Global Warming Potential
HDD	Heating Degree Days
HSS	Hollow Structural Section
HVAC	Heating, Ventilation and Air Conditioning
ICE	Individual Conditional Expectation
IDR	Interstory Drift Ratio
IES-VE	IES Virtual Environment
KNN	K-Nearest Neighbors
LCA	Life Cycle Assessment
LCC	Cycle Cost
LCCA	Life Cycle Cost Analysis
LCIA	Life Cycle Impact Assessment
LGBM	LightGBM
LOOCV	Leave-One-Out Cross-Validation
LSI	Loading Severity Index
LSTM	Long Short-Term Memory
LightGBM	Light Gradient Boosting Machine
MAE	Mean Absolute Error
MAPE	Mean Absolute Percentage Error
MDG	Mean Decrease in Gini
MDI	Mean Decrease in Impurity

ML	Machine Learning
MOO	Multi-Objective Optimization
MOPSO	Multi-Objective Particle Swarm Optimization
MSE	Mean Squared Error
N-M	Axial Force–Bending Moment Interaction
NSGA-II	Non-Dominated Sorting Genetic Algorithm II
P-Delta	P-Δ Effect
PCA	Principal Component Analysis
PDP	Partial Dependence Plot
PGA	Peak Ground Acceleration
PMV	Predicted Mean Vote
PPD	Predicted Percentage of Dissatisfied
PSA	Pseudo Spectral Acceleration
PSO	Particle Swarm Optimization
PV	Photovoltaic
RC	Reinforced Concrete
RCC	Reinforced Cement Concrete
RF	Techniques such as Random Forests
RMSE	Root Mean Square Error
RNN	Recurrent Neural Network
R^2	Coefficient of Determination
SA	Simulated Annealing
SEER	Seasonal Energy Efficiency Ratio
SHAP	Shapley Additive Explanations
SHGC	Solar Heat Gain Coefficient
SVM	Support Vector Machines
SVR	Support Vector Regression
Sa	Spectral Acceleration
Sd	Spectral Displacement
TMY	Using Typical Meteorological Year
TPOT	Tree-based Pipeline Optimization Tool
TRNSYS	Transient System Simulation
U-value	Thermal Transmittance
UMAP	Uniform Manifold Approximation and Projection
VAE	Variational Autoencoder
WWR	Window-to-Wall Ratios
XGB	Extreme Gradient Boosting
fc'	Compressive Strength of Concrete
k-Fold	k-Fold Cross-Validation
t-SNE	t-distributed Stochastic Neighbor Embedding

References

1. Heinz E, Sovacool BK, Kwan T, et al. Critically reviewing the 50 sociotechnical risks of building sector decarbonization: Conceptualizing risk as a proximity spiral. Energy and Buildings. 2025; 344: 116042. doi: 10.1016/j.enbuild.2025.116042
2. Vallati A, Di Matteo M, Sundararajan M, et al. Development and optimization of an energy saving strategy for social housing applications by water source-heat pump integrating photovoltaic-thermal panels. Energy. 2024; 301: 131531. doi: 10.1016/j.energy.2024.131531
3. Lokko M, Manu FW, Mboup N, et al. Comparing the whole life cycle carbon impact of conventional and biogenic building materials across major residential typologies in Ghana and Senegal. Sustainable Cities and Society. 2024; 106: 105332. doi: 10.1016/j.scs.2024.105332
4. Omrany H, Soebarto V. Time to do More: Realisation of Life-Cycle Net-Zero Energy Buildings. In: Abraham MA (editor). Encyclopedia of Sustainable Technologies, 2nd, ed. Elsevier; 2024. pp. 459–472.
5. Idrissi Kaitouni S, Romani Z, Jamil A, et al. Zero carbon urban buildings (ZCUBs) in the era of climate change, digital transformation and energy transition: A scoping review from 2000 to 2024. Building and Environment. 2025; 280: 113116. doi: 10.1016/j.buildenv.2025.113116
6. Ulpiani G, Yenneti K, Pigliautile I, et al. Urban heat mitigation and adaptation: the state of the art. In: Aghamohammadi N, Santamouris M (editors). Mitigation and Adaptation of Urban Overheating: The Impact of Warmer Cities on Climate, Energy, Health, Environmental Quality, Economy, and Quality of Life. Elsevier: Amsterdam, The Netherlands; 2024. pp. 23–90.
7. Jamilu G, Abdou A, Asif M. Dynamic facades for sustainable buildings: A review of classification, applications, prospects and challenges. Energy Reports. 2024; 11: 5999–6014. doi: 10.1016/j.egyr.2024.05.047
8. Jia Z, Wang M, Xiang C. Photovoltaic Trombe wall system: Multi-functional performance, optimization parameters, and evolutionary insights—A comprehensive review. Journal of Building Engineering. 2025; 115: 114536. doi: 10.1016/j.jobe.2025.114536
9. Ghasaban M, Yeganeh M, Irani M. Optimizing daylight, sky view and energy production in semi-transparent photovoltaic facades of office buildings: A comparative study in four climate zones. Applied Energy. 2025; 377(Part D): 124707. doi: 10.1016/j.apenergy.2024.124707
10. Han M, Lu L, Sun B. Overall energy performance of building-integrated bifacial photovoltaic sunshades with different installation and building parameters in hot and humid regions. Solar Energy. 2024; 275: 112619. doi: 10.1016/j.solener.2024.112619
11. Muñoz-Salcedo M, Saquinaula-Brito JL, Ortíz-Mata J, et al. A simple simultaneous envelope/system optimization for energy efficiency improvement in near-zero energy buildings. Energy Conversion and Management: X. 2025; 26: 100951. doi: 10.1016/j.ecmx.2025.100951
12. Morsy A, Kandil S, Ewais HA, et al. Eco-conscious flame retardants for enhanced fire resistance in natural fiber reinforced polymers composite: A review bio-based, and industry implications. Chemosphere. 2025; 377: 144360. doi: 10.1016/j.chemosphere.2025.144360
13. Wang M, Duan X, Li L, et al. Performance improvement of poly (lactic acid) films for bioelectronics with eco-friendly supercritical fluids combined with activated-carbon technique. Sustainable Materials and Technologies. 2023; 38: e00739. doi: 10.1016/j.susmat.2023.e00739
14. Ye F, Wei H, Xiao Y, et al. Bio-based insulation materials in sustainable constructions: A review of environmental, thermal and acoustic insulation, durability, and mechanical performances. Renewable and Sustainable Energy Reviews. 2025; 223: 115872. doi: 10.1016/j.rser.2025.115872
15. Gao X, Xiao F, Liu Q, et al. Increasing influence of compound dry-hot events on vegetation in northern China in recent years. Journal of Arid Environments. 2025; 229: 105393. doi: 10.1016/j.jaridenv.2025.105393
16. Matongo TJ, Ngock GRH, Yamb E, et al. Data on air temperature, relative humidity, and dew point in three housing modes in a building in a hot and humid area of Douala, Cameroon. Data in Brief. 2025; 63: 112120. doi: 10.1016/j.dib.2025.112120
17. Pang Y, Hao Z, Chen Y, et al. Amplified contrasts in evapotranspiration between wet and dry regions caused by compound drought-hot events. Global and Planetary Change. 2025; 255: 105108. doi: 10.1016/j.gloplacha.2025.105108
18. Panigrahi SS, Hemis M, Singh CB. Energy and moisture source-term based distributive (luikov) parameter

model to simulate rapeseed hot-air drying. Journal of Stored Products Research. 2025; 114: 102701. doi: 10.1016/j.jspr.2025.102701
19. Fu C, Tseng ML, Sethanan K. A hybrid combined cooling, heating and power system with carbon emission, economic cost and energy consumption constrains: An optimization and performance analysis. Applied Thermal Engineering. 2025; 279(Part E): 127877. doi: 10.1016/j.applthermaleng.2025.127877
20. Shu Z, Zhou Y, Liu W, et al. Multi-objective optimization approach for timber-concrete hybrid shear wall building structures considering construction cost and carbon emissions. Structures. 2025; 78: 109221. doi: 10.1016/j.istruc.2025.109221
21. Polatoğlu A. A thorough examination of concurrent measurements cosmic ray radiation and meteorological parameters with the support of machine learning. Radiation Measurements. 2025; 181: 107375. doi: 10.1016/j.radmeas.2025.107375
22. Zhou P, Qi Y, Yang Q, et al. Neural topic modeling of machine learning applications in building: Key topics, algorithms, and evolution patterns. Automation in Construction. 2025; 170: 105890. doi: 10.1016/j.autcon.2024.105890
23. Baek D, Kim H, Wei Q, et al. Evaluating the impact of windows, artificial windows, and ceiling height on stress levels through subjective and objective measures. Building and Environment. 2025; 281: 113182. doi: 10.1016/j.buildenv.2025.113182
24. Dogan A, Kayaci N, Demir H, et al. An experimental comparison of radiant wall and ceiling cooling system integrated with ground source heat pump and direct expansion fan coil system in a highly glazed office room. Energy and Buildings. 2022; 273: 112412. doi: 10.1016/j.enbuild.2022.112412
25. Cheng M, Huang Z, Zheng Y. A review on life-cycle carbon emissions of reinforced concrete buildings: Calculation and reduction. Journal of Cleaner Production. 2025; 526: 146501. doi: 10.1016/j.jclepro.2025.146501
26. Kong L, Wang L, Li F, et al. An innovative life cycle scenario-driven method for product carbon emissions prediction in the early design phase. Computers & Industrial Engineering. 2025; 209: 111461. doi: 10.1016/j.cie.2025.111461
27. Witte A, Garg N. Quantifying the global warming potential of low carbon concrete mixes: Comparison of existing life cycle analysis tools. Case Studies in Construction Materials. 2024; 20: e02832. doi: 10.1016/j.cscm.2023.e02832
28. Keshavarz A, Farajzadeh Z. Exploring the impacts of climate change on ecological footprint in Iran: A dynamic input-output analysis. Environmental Development. 2025; 55: 101217. doi: 10.1016/j.envdev.2025.101217
29. Roshan GR, Saman AA, Sarli R, et al. Projected shifts in wind energy availability in response to climate change in southwestern Iran. Sustainable Energy Technologies and Assessments. 2025; 83: 104655. doi: 10.1016/j.seta.2025.104655
30. Yaghoubi F, Bannayan M. Toward climate-resilient agriculture in Iran: Modeling quinoa viability under future climate scenarios. Agricultural Systems. 2026; 231: 104551. doi: 10.1016/j.agsy.2025.104551
31. Bian J, Yi D, Yao E, et al. Integrated assessment method for carbon emission and cost throughout the life cycle of office buildings: A comparative study of steel structure and timber structure. Structures. 2025; 77: 109103. doi: 10.1016/j.istruc.2025.109103
32. Chen Y, Han M, Liu X, et al. Assessing the environmental and economic impacts of the oyster life cycle under renewable energy expansion. Journal of Environmental Management. 2025; 389: 126220. doi: 10.1016/j.jenvman.2025.126220
33. Daoudi M, Daoudi I, Idrissi A, et al. Analyzing life cycle costs and carbon emission reduction of a first offshore wind farm in africa under the climatic conditions of Morocco: Case study. Physics and Chemistry of the Earth, Parts A/B/C. 2025; 139: 103937. doi: 10.1016/j.pce.2025.103937
34. Ren Y, Ren Z, Zou G, et al. Multi-objective optimization of capacity configuration for district heating and cooling system based on life cycle cost and annual carbon dioxide emissions. Journal of Building Engineering. 2025; 109: 113038. doi: 10.1016/j.jobe.2025.113038
35. Hasanov T, Charlier D. Classifying energy behaviors to optimize sustainability: Insights from French residential heating practices. Energy Economics. 2025; 152: 109000. doi: 10.1016/j.eneco.2025.109000
36. Rabie D, Farzaneh H. A novel modeling framework for demand response-based energy management systems in smart electricity markets, using optimization and multi-criteria decision making techniques. Applied Energy. 2026; 405: 127228. doi: 10.1016/j.apenergy.2025.127228
37. Ramsey P, Gingerich D, Best K, et al. Providing for occupant experience in optimized connected energy communities—A critical review. Building and Environment. 2024; 265: 111988. doi:

10.1016/j.buildenv.2024.111988
38. Bounnah A, Bourbia PF. Optimizing urban morphology for thermal comfort: Real-time wind-solar synchronization via Ansys Discovery and Grasshopper. Energy and Buildings. 2026; 356: 117118. doi: 10.1016/j.enbuild.2026.117118
39. Lee Y, Ng E. An adaptable framework for resilient subtropical low-income housing under future climate and predicted lifestyles: A Hong Kong case study. Energy and Buildings. 2025; 348: 116412. doi: 10.1016/j.enbuild.2025.116412
40. Albadaineh R, Fattah AAE. Assessing cooling–lighting trade-offs in a low-income Jordanian housing archetype under climate change and heat waves. Building and Environment. 2026; 288: 114040. doi: 10.1016/j.buildenv.2025.114040
41. Villada-Medina HD, Díez-Echavarría L. Unequal benefits of metro station proximity: Income-level differences in housing price effects in Medellín. Journal of Transport Geography. 2026; 131: 104571. doi: 10.1016/j.jtrangeo.2026.104571
42. Shoaib Q, Mukherjee V, Marmaridou V, et al. Development and evaluation of sustainable henequen fibre foams for thermal insulation. Materials Today Sustainability. 2025; 31: 101111. doi: 10.1016/j.mtsust.2025.101111
43. Huo D, Zhao J, Zhao Z, et al. A comprehensive life cycle cost model for high-temperature pipe insulation: Balancing heat dissipation, temperature resistance and economic benefits. Case Studies in Thermal Engineering. 2025; 73: 106492. doi: 10.1016/j.csite.2025.106492
44. Likhon RWA, Khan MAH. Simulation-based analysis of thermal bridge reduction in multi-storey residential buildings of Bangladesh using recycled plastic waste insulation. International Journal of Thermofluids. 2025; 30: 101452. doi: 10.1016/j.ijft.2025.101452
45. Marincu C, Dan D, Moga L. Investigating the influence of building shape and insulation thickness on energy efficiency of buildings. Energy for Sustainable Development. 2024; 79: 101384. doi: 10.1016/j.esd.2024.101384
46. Castrejon-Esparza NM, González-Trevizo ME, Martínez-Torres KE, et al. Optimizing urban morphology: Evolutionary design and multi-objective optimization of thermal comfort and energy performance-based city forms for microclimate adaptation. Energy and Buildings. 2025; 342: 115750. doi: 10.1016/j.enbuild.2025.115750
47. Jansen D, Richter V, Maier L, et al. Open-source framework for automated generation of building energy performance simulation models and beyond from BIM Data. Automation in Construction. 2025; 179: 106427. doi: 10.1016/j.autcon.2025.106427
48. Pan Y, Zhu M, Lv Y, et al. Building energy simulation and its application for building performance optimization: A review of methods, tools, and case studies. Advances in Applied Energy. 2023; 10: 100135. doi: 10.1016/j.adapen.2023.100135
49. Aloshan M, Aldali K. Empirical study of facade retrofits for optimizing energy efficiency and cooling in school buildings in Saudi Arabia. Energy Reports. 2024; 12: 4105–4128. doi: 10.1016/j.egyr.2024.09.076
50. Golkar S, Baneshi M, Fathi A. Effect of cool and thermal paints on the cooling and heating loads in various climates. Energy Storage and Saving. In press. 2025. doi: 10.1016/j.enss.2025.05.007
51. Hu M, Zhang K, Nguyen Q, et al. The effects of passive design on indoor thermal comfort and energy savings for residential buildings in hot climates: A systematic review. Urban Climate. 2023; 49: 101466. doi: 10.1016/j.uclim.2023.101466
52. Liu B, Li H, Song Z, et al. Wrinkled-porous core-shell SiO_2 aerogel fiber composites for thermal insulation coatings: Strain energy storage, unidirectional gas channels, and water resistance. Ceramics International. 2025; 51(28, Part B): 57355–57369. doi: 10.1016/j.ceramint.2025.09.445
53. Dong X, He BJ. A standardized assessment framework for green roof decarbonization: A review of embodied carbon, carbon sequestration, bioenergy supply, and operational carbon scenarios. Renewable and Sustainable Energy Reviews. 2023; 182: 113376. doi: 10.1016/j.rser.2023.113376
54. Xu P, Xu X. Thermal comfort, energy consumption, and carbon emissions of building envelope in office buildings: A comparative study of 46 envelope materials. Building and Environment. 2025; 285(Part C): 113578. doi: 10.1016/j.buildenv.2025.113578
55. Lv J, Lin X, Liao S, et al. Computation of vertical density distribution of compressed wood as a function of temperature, moisture content, and compression load. Construction and Building Materials. 2025; 490: 142424. doi: 10.1016/j.conbuildmat.2025.142424
56. Cornette JFP, Blondeau J. Operational greenhouse gas emissions of various energy carriers for building heating. Cleaner Energy Systems. 2024; 9: 100148. doi: 10.1016/j.cles.2024.100148

57. Srikanth A, Ramesh SJ, Heath G, et al. Democratizing life cycle assessment by developing a streamlined model of greenhouse gas emissions from US natural gas supply chains. Cell Reports Sustainability. 2025; 3(1): 100554. doi: 10.1016/j.crsus.2025.100554
58. Khan MHA, Sitaraman T, Haque N, et al. Strategies for life cycle impact reduction of green hydrogen production—Influence of electrolyser value chain design. International Journal of Hydrogen Energy. 2024; 62: 769–782. doi: 10.1016/j.ijhydene.2024.01.081
59. Alaux N, Marton C, Steinmann J, et al. Whole-life greenhouse gas emission reduction and removal strategies for buildings: Impacts and diffusion potentials across EU Member States. Journal of Environmental Management. 2024; 370: 122915. doi: 10.1016/j.jenvman.2024.122915
60. Xie M, Li J, Wei Z, et al. Multi-objective optimization for pipeline systems: A maintenance model using NSGA-II considering flow capacity and total cost. Reliability Engineering & System Safety. 2026; 266(Part A): 111663. doi: 10.1016/j.ress.2025.111663
61. Alaa H, Yehia M, Ayoub M. Metaheuristic optimization of roof designs to enhance energy performance and thermal comfort using parametrization and machine learning. Solar Energy. 2025; 286: 113186. doi: 10.1016/j.solener.2024.113186
62. Naghipour P, Naghipour A. Energy performance analysis of residential buildings in Bandar Anzali: Influence of orientation and aspect ratio. Next Sustainability. 2025; 5: 100140. doi: 10.1016/j.nxsust.2025.100140
63. Song G, Chen Y, He Y, et al. Techno-economic and life cycle greenhouse gas assessment of green ammonia produced by low-pressure Haber-Bosch process. Energy Nexus. 2025; 17: 100379. doi: 10.1016/j.nexus.2025.100379
64. Alamri S, Sadeq AM, Ayadi M, et al. Advanced optimization of a biogas-based multigeneration multi effect distillation system integrated with desalination process for enhancing sustainable energy resource efficiency: CatBoost-supported multi objective multi-verse optimization. Desalination. 2026; 619: 119514. doi: 10.1016/j.desal.2025.119514
65. Naghipour P, Naghipour A. Evaluating heating energy consumption in residential buildings using hybrid machine learning models: The case of parsabad city. Next Research. 2025; 2(3): 100721. doi: 10.1016/j.nexres.2025.100721
66. Wang C, Zhang Q, Xu X, et al. BPS-V: A blockchain-based trust model for the Internet of Vehicles with privacy-preserving. Ad Hoc Networks. 2024; 163: 103566. doi: 10.1016/j.adhoc.2024.103566
67. Yao H, Wan C. Multi-factor portfolio optimization: A combined random Forest–AdaBoost model with cost-sensitive learning. Pacific-Basin Finance Journal. 2025; 94: 102946. doi: 10.1016/j.pacfin.2025.102946
68. Mostafa Refat Ismail M, Aly Nessim A, Fathy F. Factors affecting museum buildings and heritage spaces in terms of energy optimization and comfort. Ain Shams Engineering Journal. 2024; 15(12): 103069. doi: 10.1016/j.asej.2024.103069
69. Myroniuk K, Zhelykh V, Furdas Y, et al. Energy-saving of passive ventilation systems in thermally modernized residential buildings—A review. Energy and Buildings. 2026; 350: 116681. doi: 10.1016/j.enbuild.2025.116681
70. Maaith N, Sharmin T, Bk S. Socio-technical dynamics of energy consumption in low-income housing in Amman, Jordan. Habitat International. 2025; 163: 103485. doi: 10.1016/j.habitatint.2025.103485
71. Sunikka-Blank M, Galvin R. Extending the prebound effect: The gap between healthy and actual energy consumption among low-income households in the global south. Energy Research & Social Science. 2025; 129: 104390. doi: 10.1016/j.erss.2025.104390
72. Choi BH, Song SY. Insulation performance evaluation of stone-finished exterior insulation systems with insulation frames for green remodeling of concrete exterior walls. Journal of Building Engineering. 2024; 90: 109412. doi: 10.1016/j.jobe.2024.109412
73. Naghipour P, Naghipour A, Shirdel AH, et al. Sustainability in Historical Islamic Architecture: Lessons from Sheikh Lotfollah Mosque's Construction Techniques. Journal of Islamic Architecture. 2025; 8(3): 585–603. doi: 10.18860/jia.v8i3.29053
74. Spudys P, Jurelionis A, Fokaides P. Digitizing buildings sustainability assessment: Integrating energy audits, operational energy assessments, and life cycle assessments for enhanced building assessment. Energy. 2025; 316: 134429. doi: 10.1016/j.energy.2025.134429
75. Soleimani K, Bakhshi A, Ghanian M. Voices from Iranian Farmers: Balancing livelihood and sustainability in the climate change Era. World Development Perspectives. 2025; 40: 100742. doi: 10.1016/j.wdp.2025.100742
76. Bakthavatchalam B, Al-Doori GF, Algarni S, et al. Life cycle cost analysis of an innovative nanofluid assisted photovoltaic thermoelectric air conditioner for energy efficiency enhancement in buildings. Case Studies in Thermal Engineering. 2025; 73: 106494. doi: 10.1016/j.csite.2025.106494

77. Malomo D, Xie Y, Doudak G. Unified life-cycle cost–benefit analysis framework and critical review for sustainable retrofit of Canada's existing buildings using mass timber. Canadian Journal of Civil Engineering. 2024; 51(7): 687–703. doi: 10.1139/cjce-2023-0222
78. Erdiwansyah, Mamat R, Syafrizal, et al. Emerging role of generative AI in renewable energy forecasting and system optimization. Sustainable Chemistry for Climate Action. 2025; 7: 100099. doi: 10.1016/j.scca.2025.100099
79. Ebekozien A, Aigbavboa CO, Samsurijan MS, et al. Developing a framework for housing financing: A case study of Nigeria's sustainable low-cost housing via soft system methodology. Engineering, Construction and Architectural Management. 2025; 32(13): 27–48. doi: 10.1108/ECAM-09-2023-0895
80. Naghipour P. Metaheuristic model tuning for energy forecasting in low-income housing in the MollaZeynal region of Tabriz city: Linking comfort and carbon. Next Research. 2026; 4: 101265. doi: 10.1016/j.nexres.2025.101265
81. Ouria M, Moura P, Ouria A, et al. Multi-objective architectural parametric optimization toward decarbonizing building sector—Tabriz city case study. Journal of Building Engineering. 2025; 105: 112422. doi: 10.1016/j.jobe.2025.112422
82. Luo X, Yang J, Fang Y, et al. Phased optimization of classroom units for low-carbon sustainability and occupant health. Energy. 2025; 335: 138009. doi: 10.1016/j.energy.2025.138009
83. Thibault G, Simon L, Robin G. Integrating life cycle sustainability assessment into building renovation strategies. Building and Environment. 2025; 286: 113694. doi: 10.1016/j.buildenv.2025.113694
84. Nasiri N, Rahbar N. A systematic review of thermal comfort in vernacular underground architecture of hot and arid climates: Emphasizing Iranian case studies. Energy and Buildings. 2026; 353: 116937. doi: 10.1016/j.enbuild.2025.116937
85. Kamazani MA, Dixit MK, Shanbhag SS. Multi-objective genetic optimization of embodied and operational energy and carbon impacts of buildings in current and future scenarios. Energy and Buildings. 2025; 338: 115748. doi: 10.1016/j.enbuild.2025.115748
86. Ibrahim MM, Suarez-Lopez MJ, Hanafy AA, et al. Optimizing NZEB performance: A review of design strategies and case studies. Results in Engineering. 2025; 25: 103950. doi: 10.1016/j.rineng.2025.103950
87. Asadpour F, Shirdel AH, Naghipour P. Evaluation of perceptual indicators of physical environment affecting the inducement of citizen's sense of place in urban neighborhoods. Energy and Buildings. 2024; 325: 114992. doi: 10.1016/j.enbuild.2024.114992
88. Ran J, Qiu Y, Liu J, et al. Coordinated optimization design of buildings and regional integrated energy systems based on load prediction in future climate conditions. Applied Thermal Engineering. 2024; 241: 122338. doi: 10.1016/j.applthermaleng.2024.122338
89. Pérez G, Cabeza LF. Buildings life cycle assessment. In: Abraham MA (editor). Encyclopedia of Sustainable Technologies, 2nd ed. Elsevier; 2024. pp. 427–445.
90. Chen X, Yang H, Zhang W. Simulation-based approach to optimize passively designed buildings: A case study on a typical architectural form in hot and humid climates. Renewable and Sustainable Energy Reviews. 2018; 82(Part 2): 1712–1725. doi: 10.1016/j.rser.2017.06.018
91. Ye J, Yang F. Towards multi-scale and context-specific heat health risk assessment: A systematic review. Sustainable Cities and Society. 2025; 119: 106102. doi: 10.1016/j.scs.2024.106102
92. Ruan D, Fan C, Hu M, et al. Building-integrated photovoltaics through multi-physics synergies: A critical review of optical, thermal, and electrical models in facade applications. Renewable Energy. 2025; 251: 123332. doi: 10.1016/j.renene.2025.123332
93. Abdalla A, Islam MD, Janajreh I. Influence of building orientation on cooling load: A comparative study. International Journal of Thermofluids. 2025; 27: 101244. doi: 10.1016/j.ijft.2025.101244
94. Arul Babu ADC, Srivastava RS, Rai AC. Impact of climate change on the heating and cooling load components of an archetypical residential room in major Indian cities. Building and Environment. 2024; 250: 111181. doi: 10.1016/j.buildenv.2024.111181
95. Borelli D, Cavalletti A, Cavalletti P, et al. A methodology to evaluate the optimal insulation thickness for heating and cooling needs in different climatic zones for buildings made of reinforced concrete with cavity walls. Heliyon. 2024; 10(10): e30653. doi: 10.1016/j.heliyon.2024.e30653
96. Chaudhary GQ, Hu Z, He S, et al. Analysis of building-integrated solar desiccant air cooling systems considering the dynamic sensible and latent cooling loads. International Journal of Refrigeration. 2026; 181: 111–125. doi: 10.1016/j.ijrefrig.2025.10.007
97. Bamdad K. Cool roofs: A climate change mitigation and adaptation strategy for residential buildings. Building and

Environment. 2023; 236: 110271. doi: 10.1016/j.buildenv.2023.110271
98. Jia S, Weng Q, Yoo C, et al. Global investigation of pedestrian-level cooling and energy-saving potentials of green and cool roofs in 43 megacities. Energy and Buildings. 2025; 337: 115671. doi: 10.1016/j.enbuild.2025.115671
99. Lu M, Zeng L, Li Q, et al. Quantifying cooling benefits of cool roofs and walls applied in building clusters by scaled outdoor experiments. Sustainable Cities and Society. 2023; 97: 104741. doi: 10.1016/j.scs.2023.104741
100. Zhou J, Fang Z, Yin G, et al. Automated roof segmentation for assessing urban scale energy performance and indoor thermal environment of photovoltaic and green roofs. Energy. 2025; 338: 138958. doi: 10.1016/j.energy.2025.138958
101. Gong Q, Ding W, Liu X, et al. Multi-objective optimization framework for the building envelope of public rental housing in China's cold regions. Journal of Building Engineering. 2025; 104: 112261. doi: 10.1016/j.jobe.2025.112261
102. Qiu Z, Yong Q, Wang J, et al. A multi-objective optimization framework for performance-based building design considering the interplay between buildings and urban environments. Energy Conversion and Management. 2024; 315: 118793. doi: 10.1016/j.enconman.2024.118793
103. Wang W, Zhu L, Zhang T, et al. Integrating local climate considerations into dormitory energy optimization: An explainable machine learning and multi-objective design approach. Urban Climate. 2025; 64: 102629. doi: 10.1016/j.uclim.2025.102629
104. Epelde L, Mendizabal M, Gutiérrez L, et al. Quantification of the environmental effectiveness of nature-based solutions for increasing the resilience of cities under climate change. Urban Forestry & Urban Greening. 2022; 67: 127433. doi: 10.1016/j.ufug.2021.127433
105. Li J, Jian R, Bao S, et al. Quantifying the impact of building layouts on wind–thermal environments: A computational fluid dynamics-based approach for optimizing plans and designs in high-temperature, low-wind regions. Results in Engineering. 2025; 26: 104740. doi: 10.1016/j.rineng.2025.104740
106. Lopez-Cabeza VP, Alzate-Gaviria S, Diz-Mellado E, et al. Albedo influence on the microclimate and thermal comfort of courtyards under Mediterranean hot summer climate conditions. Sustainable Cities and Society. 2022; 81: 103872. doi: 10.1016/j.scs.2022.103872
107. Eloranta V, Inkeri E, Luoranen M, et al. Balancing trade-offs in Nordic smart local energy systems: Multi-objective and multi-criteria optimization for cost, emissions, and self-sufficiency. Renewable Energy. 2025; 257: 124696. doi: 10.1016/j.renene.2025.124696
108. Khaled B, Abdelaziz AY, Attia MA, et al. Assessing the impact of climate change on wind energy penetration: Optimization of scheduling and carbon emission analysis. Electric Power Systems Research. 2025; 248: 111929. doi: 10.1016/j.epsr.2025.111929
109. Liu T, Zhu H, Shen Y, et al. Carbon-friendly design method of tunnel lining segments based on Pareto optimal analysis. Tunnelling and Underground Space Technology. 2025; 161: 106602. doi: 10.1016/j.tust.2025.106602
110. Wu Y, Zhong L. Assessing the affordability and independence of building-integrated household green hydrogen systems in Canadian urban households under climate change. Energy Conversion and Management. 2025; 346: 120432. doi: 10.1016/j.enconman.2025.120432